

Ground improvement techniques applied to very soft clays: state of knowledge and recent advances

Marcio de Souza Soares de Almeida¹ , Maria Esther Soares Marques² , Mario Riccio^{3#} ,
Diego de Freitas Fagundes⁴ , Bruno Teixeira Lima^{5,6} , Uberescilas Fernandes Polido⁷ ,
Alessandro Cirone⁸ , Iman Hosseinpour⁹ 

Review Article

Keywords

Ground improvement
Granular columns
Cementitious binders
Geosynthetics
Settlements
Soft clays

Abstract

Soft ground improvement techniques have evolved substantially in Brazil in recent years. However, their application in soft and very soft clays requires a good understanding of the fundamentals of ground improvement techniques suited to the problem as well as the actual field behavior when implemented on a real scale. This paper describes some of the most widely used ground improvement techniques in the context of very soft clays in Brazil. The techniques described in the paper use prefabricated vertical drains (PVD) such as vacuum preloading; or combine PVD and rigid inclusion, such as CPR grouting; or are purely column-like elements such as piled embankments (including those executed with the deep mixing technique, *DSM*); or combine column-like elements with the drainage function, such as stone columns and geosynthetic encased columns; or use cementitious binders such as shallow soil mixing. The paper reference condition is a soft clay foundation in which no strengthening is implemented, such as, an embankment with basal reinforcement or soft clay with vertical prefabricated drains, or the use of vacuum preloading to speed up the consolidation rate. The applications of the ground improvement techniques are illustrated by case histories, numerical analyses, or physical models. Different types of measurements are used to evaluate the performance of each technique, including settlements, horizontal displacements, excess pore pressures, embankment applied stresses, stress concentration factors, and clay strength following the ground treatment. The settlement improvement factor β , the ratio between the settlements for untreated and treated conditions, is shown to be a suitable parameter to assess the degree of improvement imposed in the soft foundation by ranking the various methods in increased order of strengthening effect.

1. Introduction

Soft soils may require the construction of an embankment in stages, which may lengthen the overall construction time excessively even when prefabricated vertical drains (*PVD*) are used to accelerate settlements (Almeida et al., 2008). In the case of very soft soils, basal geosynthetic reinforcement and lateral berms may also be necessary in order to maintain stability.

A possible design constraint is that post-construction residual (secondary) settlements must be negligible. However,

achieving this goal requires a greater embankment thickness so that secondary settlements occur in the form of primary settlements during construction.

Large fill volumes can make the technique of staged construction with *PVDs* and reinforcement unfeasible, especially in the case of very thick compressible layers. In order to overcome these issues, the embankment may be supported by column-like elements (Almeida & Marques, 2013) or the soft ground may be improved by cementitious binders (e.g., Lemos et al., 2020). The present article discusses these ground improvement techniques as carried out in Brazil over

#Corresponding author. E-mail address: mvrfl1000@gmail.com

¹Universidade Federal do Rio de Janeiro, Civil Engineering Program, Rio de Janeiro, RJ, Brasil.

²Instituto Militar de Engenharia, Fortification and Construction Department, Rio de Janeiro, RJ, Brasil.

³Universidade Federal de Juiz de Fora, Graduate School of Civil Engineering, Juiz de Fora, MG, Brasil.

⁴Universidade Federal do Rio Grande, School of Engineering, Rio Grande, RS, Brasil.

⁵Universidade do Estado do Rio de Janeiro, RJ, Brasil.

⁶Universidade Federal Fluminense, Niteroi, RJ, Brasil.

⁷GEOCONSULT, Vitória, ES, Brasil.

⁸Pontifícia Universidade Católica do Rio de Janeiro, Department of Civil and Environmental Engineering, Rio de Janeiro, RJ, Brasil.

⁹University of Guilan, Faculty of Engineering, Civil Engineering Department, Rasht, Guilan, Iran.

Submitted on July 26, 2022; Final Acceptance on November 14, 2022; Discussion open until May 31, 2023.

<https://doi.org/10.28927/SR.2023.008222>



This is an Open Access article distributed under the terms of the Creative Commons Attribution License, which permits unrestricted use, distribution, and reproduction in any medium, provided the original work is properly cited.

the last decade by presenting representative field case studies, complemented by physical and numerical modeling studies. The topics covered by this paper reflect basically the work of researchers at COPPE-UFRJ, including collaborations with authors from other institutions. The article is an updated written version of the Keynote Lecture presented at the XVI PCSMGE 2019 (Almeida, 2019) which in turn was based on the 2015 Coulomb Lecture (Almeida, 2015).

2. Background

Very soft clay soils may be characterized by the number of blow counts, measured by the standard penetration test, N_{SPT} lower than 2, undrained strength S_u lower than 20 kPa, and point resistance q_c lower than 1 MPa. These soils are found in many parts of the world as well as along the Brazilian coast where the case histories presented in this paper are located.

Data from sites located to the west of the city of Rio de Janeiro (Baroni & Almeida, 2017, 2022) is presented in the plasticity chart in Figure 1. This chart shows that the range of liquid limit w_L and plasticity index PI values for these sites is far greater than those found in classic text books.

Figure 2 presents data from a stage-constructed embankment with *PVDs*, reinforcement and berms built on an extremely soft clay deposit located west of Rio de Janeiro City. The “as built” line shows that the embankment reached a total height of about 6 m with settlements of around 2.5 m over a period of 20 months. Therefore, the net embankment height is just over 3 m, even though 6 m of fill have been applied. As such large volumes of fill and long construction times are not always feasible in practice, other soft ground improvement techniques have been developed to overcome these issues

Figure 3 compares the normalized embankment stress q versus normalized δ settlement curves for the ground improvement techniques discussed in this paper, where S_u is the average undrained clay strength, H is the embankment height, and 5 and 3 shown in the horizontal axis indicate limit state and serviceability state conditions respectively for the unreinforced embankment.

The curves presented in Figure 3 show that the efficiency of the ground treatment method increases (greater loads with less settlement) as its foundation is reinforced or becomes stiffer, either by column-like elements or by adding cementitious binders to the soft soil. As shown in Figure 3, the basal geosynthetic reinforcement procedure is often included in all column-like techniques as it allows better load transfer to the column, in addition to improving stability. The basal reinforcement is indicated by dashed lines under the embankments.

In the following sections of the paper the ground improvement techniques presented in Figure 3 are analyzed. First, the unreinforced embankment (*UE*) built on soft soil, associated with the use of vacuum preloading (vacuum consolidation) to accelerate settlements, is presented as the

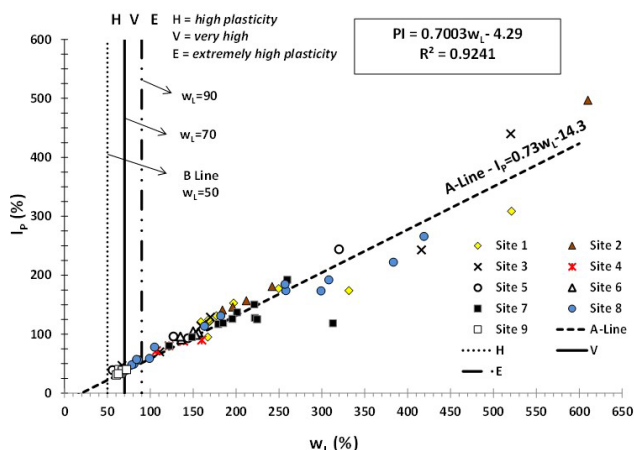


Figure 1. Plasticity chart data for 9 sites west of the city of Rio de Janeiro (Baroni & Almeida, 2017).

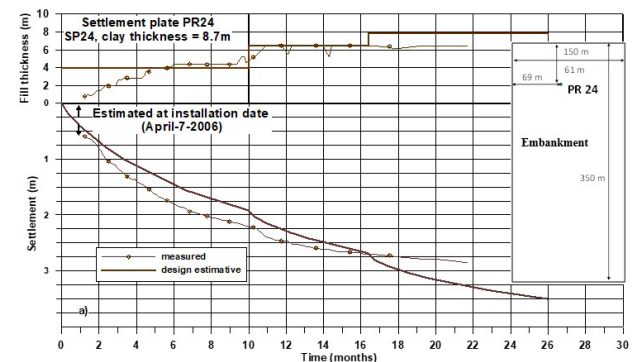


Figure 2. Stage-constructed embankment with *PVDs*, reinforcement and berms on an extremely soft soil (Almeida et al., 2008).

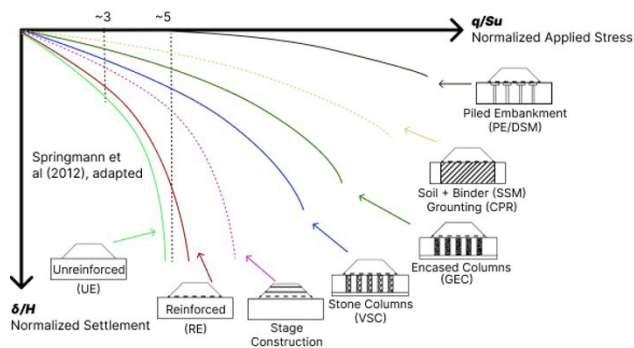


Figure 3. Normalized embankment stresses versus normalized settlements for different ground improvement techniques (adapted from Springman et al., 2012).

reference technique. Then, two techniques using granular columns are discussed: the stone column with vibro replacement (*VSC*), and the geosynthetic encased granular column (*GEC*), which includes a comparison between the *GEC* with a reinforced embankment (*RE*). The next section

describes the more efficient piled embankment method (*PE*), a column-like alternative in which piles may be driven or executed in situ by means of the deep soil mixing technique (*DSM*), which is also briefly explained. The last three sections of the paper elaborate on three ground improvement techniques that incorporate a cementitious binder, including shallow soil mixing (*SSM*), *CPR* grouting, and the aforementioned *DSM* technique.

An important parameter used in the paper is the settlement improvement factor β proposed by Priebe (1995) for the design of granular stone columns executed by vibro substitution. The parameter β is defined by the ratio between the unimproved soil settlement Δh and the settlements of the soil-column system Δh_c .

$$\beta = \frac{\Delta h}{\Delta h_c} \quad (1)$$

The concept of settlement improvement factor, is expanded here to be applied to other ground improvement techniques as well and results will be summarized in a final section.

3. Vacuum preloading

The vacuum consolidation technique for soft soil improvement, although idealized by Kjellman (1952) in the 1950s, was used more broadly worldwide only in the 1980s to enable preloading in compressible soils. The method involves applying a vacuum to a clay deposit by means of a pumping system in association with grids of drains. Its application reduces pore pressure related to the atmospheric pressure (≈ 100 kPa), promoting radial flow, increasing effective stress and accelerating settlement over time.

3.1 Membrane and drain-to-drain techniques

The vacuum consolidation technique was first designed with an airtight membrane and later without the membrane, in a system called drain-to-drain method (Figure 4).

In the vacuum system with membrane, water and air are pumped inside a pump container where pressure is close to -1 atm (Figure 4a). The vacuum pressure is applied to the horizontal drains and the sand layer (encapsulated by an impervious membrane) and thus at the top of vertical drains (*PVDs*). The membrane is stretched until it reaches the water table inside the peripheral trench, thus confining the vacuum inside the soil mass (Marques & Leroueil, 2015). The vacuum is usually measured under the membrane and during vacuum preloading, a conventional embankment can be built to accelerate settlements after the air-tightness of the membrane has been confirmed.

Drain-to-drain vacuum preloading consists of applying suction inside the soft soil layer by *PVDs* linked to a pump system by airtight collector tubes (Figure 4b) (Freitas, 2021;

Cardoso, 2021). In this case, the collectors are installed in lieu of the membrane and horizontal drains, and the *PVDs* are connected to the collectors as shown in detail in Figure 4c. A conventional fill can be carefully constructed above the connectors and collector tubes after the air-tightness of the system has been checked.

Both methods have advantages and disadvantages: the main disadvantage of vacuum system with membrane is in case of sandy layer inside the soft soil deposit, which would lower the efficiency, and for the drain-to-drain is the low efficiency usually observed in field.

The number of pumps used for vacuum preloading depends on the area size and site conditions, and drain spacing is designed to consolidate the clay deposit within a four- to six-month period. Once the proposed degree of consolidation has been achieved, the pumping is stopped and the fill height can be increased to final grade, without post-construction settlements.

The efficiency of the vacuum system with membrane is determined by the pressure applied to the deposit related to the atmospheric pressure of about 100 kPa. Thus, considering a system efficiency of 70 to 75%, the load applied by vacuum corresponds to a stress increase of about 70 - 75 kPa, approximately the load of a 4 m high embankment applied in a single step.

In the drain-to-drain system, when there is loss of suction, it is faster to repair a vacuum line due to damage, since the vertical drains are connected in lines independent of each other and the rest of the system continues to run without interruption. However, the main disadvantage of the drain-to-drain system is the connections, where leakage can occur. Also, during the consolidation process, excessive deformations can occur, so the horizontal pipes can suffer damage and interrupt the vacuum supply to the *PVDs*. Therefore, it is necessary to leave a slack in the length of the pipes.

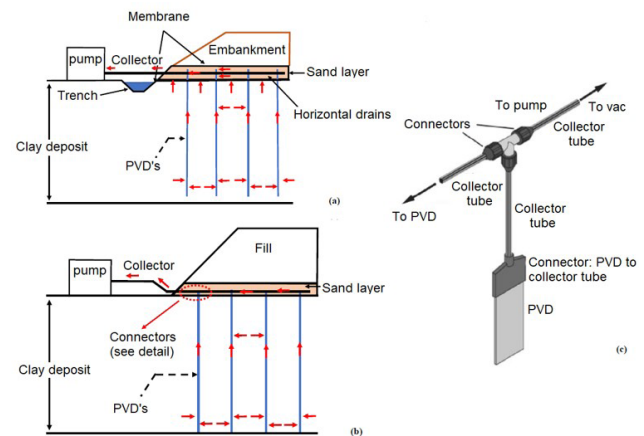


Figure 4. Vacuum consolidation technique: (a) with membrane (b) drain-to-drain (membraneless) (c) detail of connectors in the drain to drain configuration (adapted from Freitas, 2021).

While efficiency of a membrane system can be 70-75% (Marques & Leroueil, 2015), the efficiency of the drain-to-drain method is lower. López-Acosta et al. (2019), when using pressure gauges at the end of the drain-to-drain line at a site in Mexico, reported a loss of vacuum along the horizontal pipes in the order of 30%, which is equivalent to 40 to 50 kPa of pressure. The leakage associated with the drain-to-drain method is a well-known disadvantage.

New forms of vacuum application, such as the dehydration of fluid materials, have also been used in hydraulic landfills and/or soft soils on the seabed in offshore conditions (Harvey, 1997).

3.2 Vacuum preloading test and horizontal displacements

A full-scale vacuum preloading test was performed for an embankment construction on a Canadian structured clay deposit at Saint-Roch-de-l’Achingan (Marques & Leroueil,

2015) presented in Figure 5a. A plane strain finite element analysis was carried out (Almeida et al. 2021) in which the structured soft clay behavior was simulated with the *S-CLAYIS* constitutive model, but also with the Modified Cam-clay model. It is worth presenting in particular the numerical and measured results of horizontal displacements (see Figure 5b) for points *B* and *C* at inclinometer *IA1*. The numerical values ranged from 0.01 m to -0.04 m and field measurements indicated zero horizontal displacements. Therefore, numerical calculations and observed values of horizontal displacements are quite small and overall, in good agreement. The applied load was about 60% vacuum and 40% embankment loading which, according to the literature (Indraratna, 2010), results in negligible horizontal displacements, consistent with the present observed values. Settlements at the axis of the embankments were about 0.26 m stabilized around 5 months were in good agreement with numerical calculations using the *S-CLAYIS* model but were overpredicted by the Modified Cam-clay model.

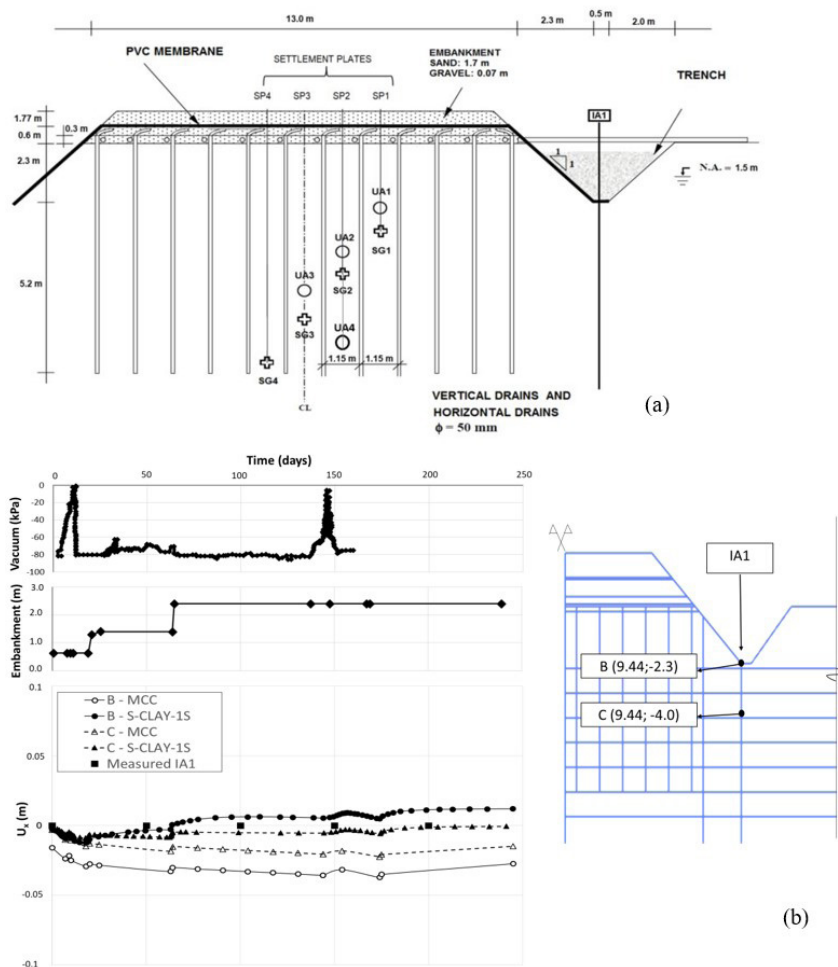


Figure 5. (a) Saint-Roch-de-l’Achingan embankment test cross section and instrumentation. (Marques & Leroueil, 2015); (b) Variation over time for vacuum pressure, embankment thickness and horizontal displacements U_x (field and numerical values) at points *B* and *C* at inclinometer *IA1* (Almeida et al. 2021).

Legend: SP = settlement plates; SG = tassometer; IA = inclinometer; UA = piezometer.

3.3 Advantages and disadvantages of the vacuum preloading

The vacuum preloading technique is widely used worldwide and has shown excellent results when applied to the improvement of soft soils, in order to reach a shorter deadline, lower fill volumes, and smaller horizontal displacements (Choa, 1989; Qian et al., 1992; Jacob et al., 1994; Rujikiatkamjorn et al., 2007; Marques & Leroueil, 2015; Zheng et al., 2017; Chai et al., 2013; Almeida et al., 2021). This section presents advantages and disadvantages of the vacuum preloading method applied to both membrane and drain-to-drain techniques.

The advantages of vacuum preloading when compared with a conventional embankment over soft soils are (Marques & Leroueil, 2015; López-Acosta et al., 2019):

- The applied vacuum load is unaffected by submersion, although the conventional fill associated with the vacuum system can be submerged, depending on settlement values;
- Earthwork volumes are lower: no berm or backfill material is required to provide preloading;
- Horizontal displacements are much smaller than those of a conventional fill, as exemplified in Figure 5b;
- Unlike traditional embankment loading, vacuum application does not cause rupture even when combined with embankment loading, although stability analysis should be carried out. Stress paths analyzed next complement this statement.

Effective stress paths (*ESP*) below conventional embankments are directly related to the location of the points in the clay foundation. For points under the embankment slope the *ESP* moves almost vertically towards the failure line as

loading progresses (Marques & Leroueil, 2015). However, as the points approach the embankment centerline the *ESP* moves away from the failure line approaching the K_0 line.

Stress paths at mid depth in the clay foundation are now assessed for the test embankment mentioned in Figure 5, a combination of vacuum and embankment loading, 60% and 40% of the total applied load respectively, as mentioned previously. Figure 6 shows the *ESP* in red lines (the numbers indicated refer to the loading stages) numerically calculated at two points located at mid depth in the clay foundation, point A located at the embankment centerline, and point B located under the embankment slope (Figure 6a). The p' - q plot in Figure 6b shows the yield curve for each point together with the critical state line and K_0 line. The stress paths of both points, A and B, presented show that the two stress paths remained fairly close to the K_0 line. Therefore, unlike traditional embankment loading, the *ESPs* when vacuum preloading is used are close to or below the K_0 line, even for points away from the embankment centerline.

The disadvantages of vacuum preloading are:

- Vacuum requires pump maintenance and there is a high energy expenditure during the pumping period, thus is not suitable for small areas;
- Higher clogging of *PVD* with vacuum;
- Vacuum loss along the length of the drain, thus a lower consolidation with depth which can lead to high post-construction settlements;
- In cold regions pumping systems cannot be used under extremely low temperatures, unless the hydraulic system is protected against freezing;
- The membrane must be airtight and vacuum efficiency decreases in clay deposits with granular layers. In

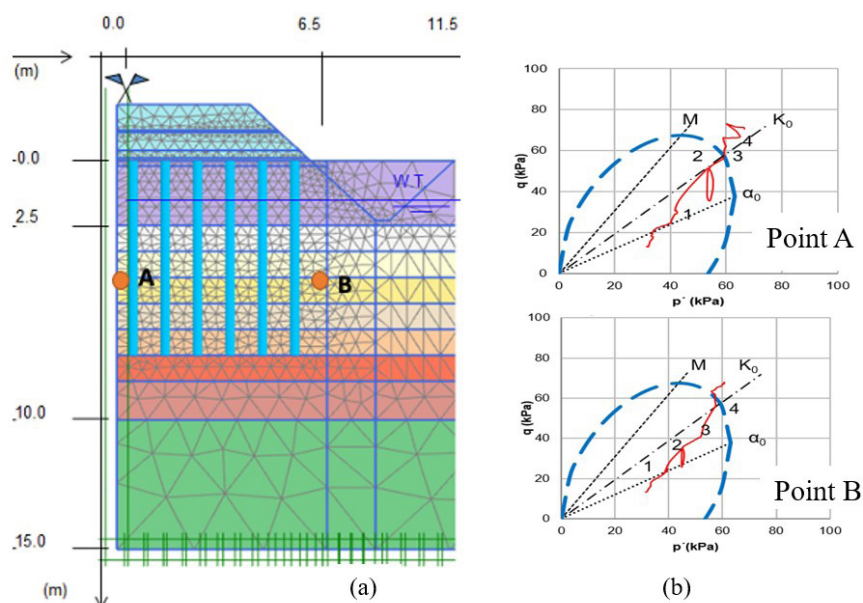


Figure 6. Numerical analysis: (a) FE mesh and points analyzed; (b) Stress paths at points A and B.

- addition, in the case of a high permeable layer at the surface, the membrane must reach greater depths;
- Vacuum pumping, when using a membrane system, increases the reference water level from the natural water table level to the level of the horizontal drains where the vacuum is applied. The case history shown in Figure 6 had a lower water table, and even though the pressure measured with the vacuum meter inside the sand layer was 80 kPa, the actual vacuum pressure installed in the clay layer was lower than the 80 kPa measured by the piezometer, as pore pressure measurements showed (Marques & Leroueil, 2015).

3.4 Vacuum preloading in the city of Rio de Janeiro

The drain-to-drain vacuum preloading technique in conjunction with a physical embankment load was used for the first time in Rio de Janeiro city for a residential project on very soft soil (Freitas, 2021; Cardoso, 2021). The vacuum preloading system consisted of 24 pumps (VP-1 to 24), working nonstop for periods between 7.5 and 9.0 months,

as shown in Figure 7. *PVDs* were installed in a triangular mesh pattern with 1.3 m spacing (Figure 8a) connected to pumps by a collector system (Figure 8b). The embankment thickness was in the range of 3.9 and 6.3 m, including the working platform (Figure 8c).

The site was composed of very soft organic dark gray clay, 8 to 15 m thick, with the occasional occurrence of shell fragments. The bulk weight of the clay (γ) varied between 11.5 and 12.5 kN/m³ and the natural water content from 191 to 242%. The soil grain size fraction was: 46% clay, 48% silt and 6% of fine sand and medium sand, resulting in a mean activity value of 2.89. The plasticity index was between 103 and 174%, thus highly compressible organic silty clay.

Eighteen settlement plates were distributed across the 5 areas and yielded settlements between 1.0 and 2.5 m. Figure 9 shows settlements measured by settlement plate *SP-03* compared with settlements curves calculated for 30 kPa and 70 kPa vacuum load. Although the vacuum pressure measured at the pumps was around 80 kPa, the measured settlements indicated that the actual applied vacuum pressure was closer to 30 kPa (Freitas, 2021; Cardoso, 2021).

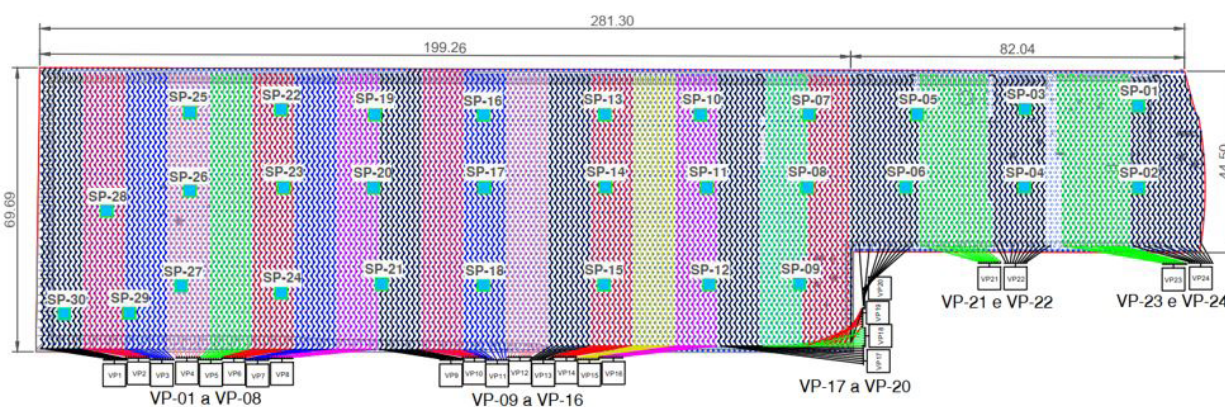


Figure 7. Vacuum application layout and settlement plates location (Freitas, 2021).

Legend: VP = vacuum pumps; SP = settlement plates.

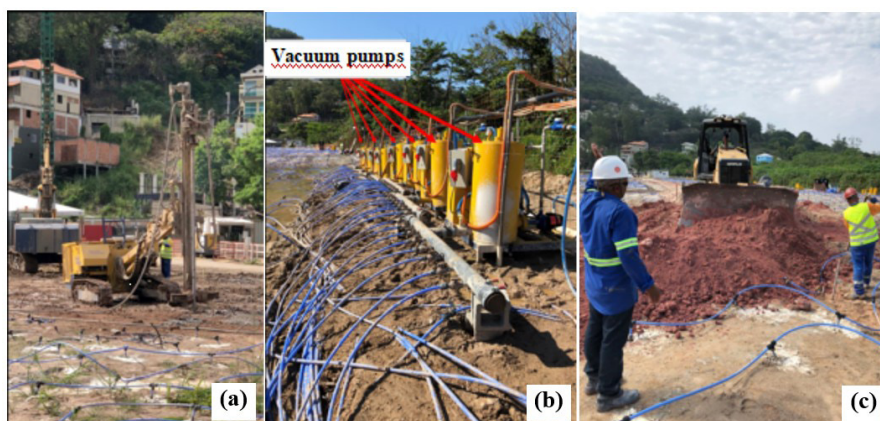


Figure 8. Drain-to-drain vacuum consolidation: (a) vertical drains and installation of collectors (b) pumps and collector tubes (c) detail of embankment construction over collectors and connections (Freitas, 2021).

Data collected from electric piezometers did not exhibit the expected decrease with time in pore pressure due to application of the vacuum, to a maximum expected value of -70kPa. However, the increase of pore pressure was evident at each stage of embankment heightening, thus the piezometer was responding to changes in stress due to heightening.

The increase in effective stress calculated due to the increase in embankment height was around 90 kPa. However, piezocone tests carried out after the vacuum was turned off showed an increase of only 5 kPa of undrained strength in 3 *CPTus*. This increase may be related to an increase in the effective stress of approximately 20 kPa, and more consistent with an applied vacuum pressure of close to 30 kPa.

Results from settlement plates, piezometers and *CPTus* showed that the effective stress increase due to vacuum was lower than 30kPa, thus a low efficiency at this site. The connections with the PVD's and the horizontal pipes are the weak points in the vacuum system, where leakage can occur, thus it is imperative vacuum pressure monitoring in horizontal drain lines, at the end of the horizontal tubes, farthest from the vacuum pump. With this procedure, it is possible to make corrections to ensure maximum pressure, check the efficiency of the system and identify possible damage that could generate the loss of pressure along the line. Further field research to monitor pressures along the drain is needed to obtain the actual efficiency.

3.5 Final remarks

The main lessons learned about vacuum preloading were:

- The thickness of the working platform can be a decisive factor in terms of the embankment stability due to the low initial value of S_u ;
- The connections between the PVDs and the horizontal pipes can be the weak points in the drain-to-drain vacuum system, where leakage can occur, thus it is essential to monitor vacuum pressure in the horizontal drain lines at the end of the horizontal tubes, farthest from the vacuum pump.

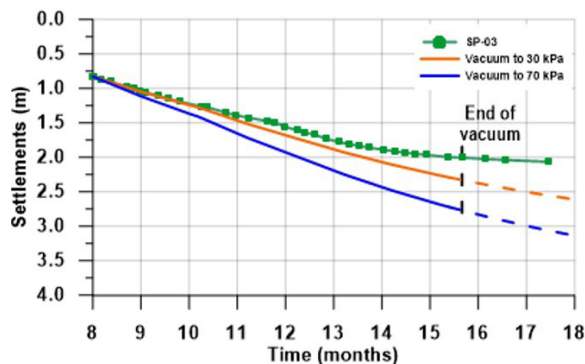


Figure 9. Settlement values measured at *SP03* and settlement predictions for vacuum of 30 kPa or 70 kPa.

4. Vibro substitution with stone columns (VSC)

Stone columns are used to increase bearing capacity, reduce settlements and increase the consolidation rate. Ground improvement with granular columns involves the replacement of 10% – 50% of compressible soil, by area, with a granular material such as gravel (crushed rock), or sand (FHWA, 1983).

4.1 Design methods

Due to its simplicity, Priebe's (1995) method for stone column design is widely used to obtain the settlement improvement factor β (named n_o by Priebe, 1995). McCabe et al. (2009) reported good agreement between measured and computed values of β given by Priebe's method, as illustrated in Figure 10. Studies carried out in Brazil are also included in Figure 10 (Lima, 2012; Sandroni, 2014; Saboya et. al, 2021; Riccio Filho et al., 2022), showing that, overall, the values are relatively close to the range of values obtained for other studies.

Another important parameter in ground improvement in general is the area replacement ratio (α) defined as the ratio between the area of a column A_c and its area of influence A :

$$\alpha = \frac{A_c}{A} \quad (2)$$

where $A_c = \pi \cdot d_c^2/4$ is the cross-section area of a column; d_c is the column diameter; $A = s^2$ (for square mesh); s is the column spacing, or more generally, $A = \pi \cdot d_e^2/4$; d_e is the diameter of the unit cell; $d_e = 1.13 \cdot s$ (square mesh); or $d_e = 1.05 \cdot s$ (triangular mesh, less often adopted). The column diameter d_c is a direct function of the average value of the undrained strength of the soft clay (Besançon et al., 1984). The soft clay sites studied here have a typical value of undrained strength S_u around 10 kPa, for which the column diameter d_c is in the range of 0.90 m to 1.0 m.

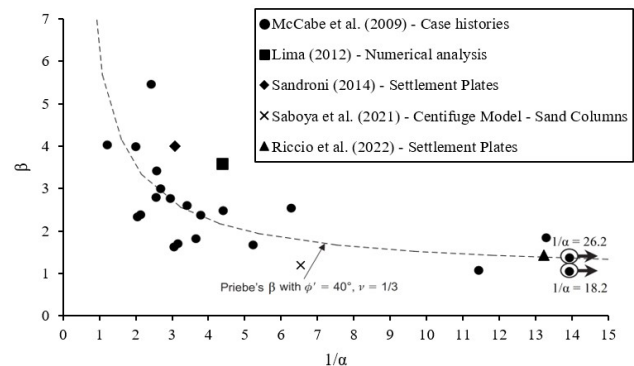


Figure 10. Settlement reduction factor versus inverse of area replacement ratio (see McCabe et al., 2009 for the other case histories).

$$d_c (cm) = 120 - 1.4S_u (kPa) \quad (3)$$

The stability analysis of embankments built on vibro stone columns (VSC) is usually performed using composite ground parameters (Priebe, 1995), which include the strength and specific weight parameters of the soft clay and the granular column. Stability analysis of a test area with VSC are illustrated by Riccio Filho et al. (2022), and a summary of their results are presented below.

Among the several methodologies proposed to predict the settlement rate of an embankment on VSC, the approach presented by Han & Ye (2002) is the most widely used. However, consistent analysis may be also obtained using the simple Barron (1948) theory (Riccio Filho et al., 2022).

4.2 Brazilian studies on stone columns applications

The vibro-replacement technique was implemented in Brazil in the mid-2000s, with several additional projects carried out since then, some highlighted next.

4.2.1 Stockyard test area

The first study reported here is related to a test area executed at the TERNIUM stockyard located in Itaguaí, State

of Rio de Janeiro (Almeida et al., 2014). The test area was configured in an 8 x 8 square mesh/grid, with 1.85 m spacing. The stone column diameter was 1.0 m (replacement ratio $a_c = 23\%$) and the length was 11.25 m, as shown in Figure 11.

The geotechnical profile is composed by a soft soil layer, about 6.0 m thick, a 2.6 m thick sand layer below, and another soft clays layer, about 3 m thick. The remaining soil profile consisted mainly of sand layers, quite often without continuity. Table 1 summarizes the parameters obtained from samples taken in the three clay layers.

Table 1. Soil parameter values for clay layers 1 to 3 (Almeida et al., 2014).

Parameters	Layer 1	Layer 2*	Layer 3*
C_c	1.59	1.07	1.00
C_s	0.27	0.13	0.12
e_0	3.11	1.91	1.90
c_v [m^2/s] $\times 10^{-8}$	2.50	4.45	4.45
OCR	2.7	1.2	1.2
γ [kN/m^3]	13.3	15.5	15.5
ϕ' [degrees]	25.0	25.0	25.0

*Data from Marques et al. (2008). C_c = compression index; C_s = swelling index; e_0 = initial void ratio; c_v = coefficient of consolidation; OCR = overconsolidation ratio, γ = soil unit weight; ϕ' = friction angle

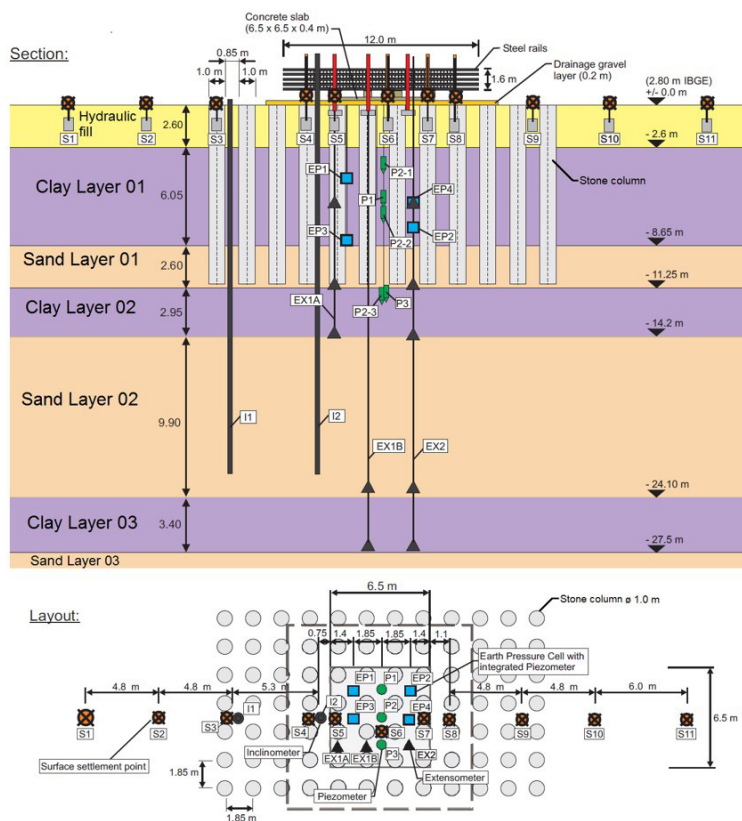


Figure 11. Layout of the test area and instrumentation (Almeida et al., 2014).

Legend: S = Surface settlement point; EP = Earth pressure cell with integrated piezometer; EX = Extensometer; I = Inclinometer; P = Piezometer.

The field instrumentation (Figure 11) included eleven settlement plates (*S*), two inclinometers (*IN*), nine vibrating wire piezometers (*PZ*) and four horizontal stress cells (*EP*).

Two- and three-dimensional finite element analyses were carried out (Roza, 2012; Almeida et al., 2014), in which the soft soil layers were simulated with a Cam-Clay type model, and the Mohr Coulomb model was used for the other layers. A study was performed to assess the earth pressure coefficient after stone column installation, K^* , and the best fit between numerical results and field measurements was provided using $K^* = 1.25$, which is close to the values presented in the literature (Almeida et al., 2014).

The results of the 2D analysis (FEM 2D) presented for comparison with field measurements are the vertical displacements (inside and outside the loaded area) and horizontal displacements, at Inclinometer *I2*, (Figure 12), excess pore-pressure (Figure 13) and horizontal stresses (Figure 14). Differences between numerical predictions and measurements of the vertical and horizontal displacements increased after the 22nd day, when the limit state condition

was observed, close to failure, which was not adequately modelled in the numerical analyses (Almeida et al. 2014).

4.2.2 Ore piles in the stockyard area

Based on the good results of the test area, further numerical analyses were performed for the ore piles in the stockyard in which the area replacement ratio was 16% (Lima et al., 2019). Figure 15 presents the instrumentation installed at the section of study in the Stockyard, with two horizontal profilometer gauges (HPG), eight settlement sensors (SS) and piezometers (PZ), and the geotechnical profile.

Figure 16 shows the settlements measured by the *SS-N3* (northern part) and the northern *HPG*, together with results of 2D finite element analysis (FE). The average vertical stresses applied by the northern stack of pellets of ore are also plotted. The results show that the numerical analysis provided a good prediction of the settlement measured by settlement sensors and the profilometer. The same constitutive models and soil parameters from the test area were used in the stockyard.

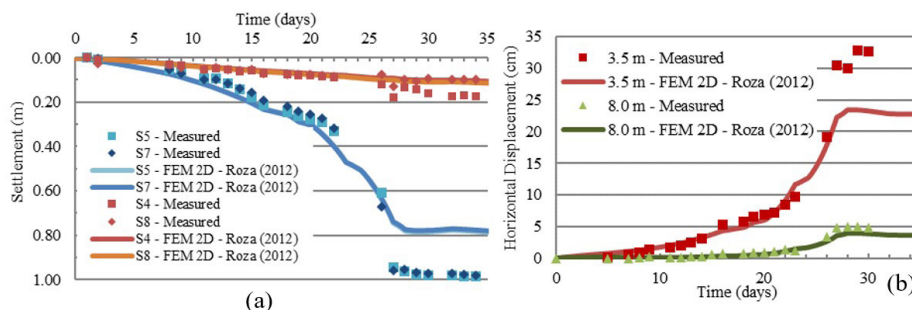


Figure 12. Vertical (a) and horizontal – Inclinometer *I2* (b) displacements at instrumentation (Almeida et al., 2014).

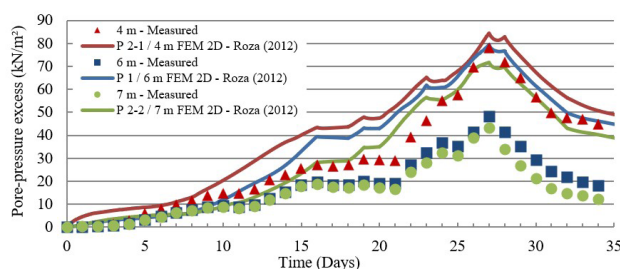


Figure 13. Excess pore-pressure (Almeida et al., 2014).

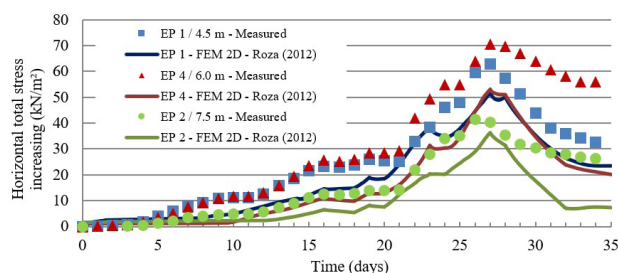


Figure 14. Horizontal stress (Almeida et al., 2014).

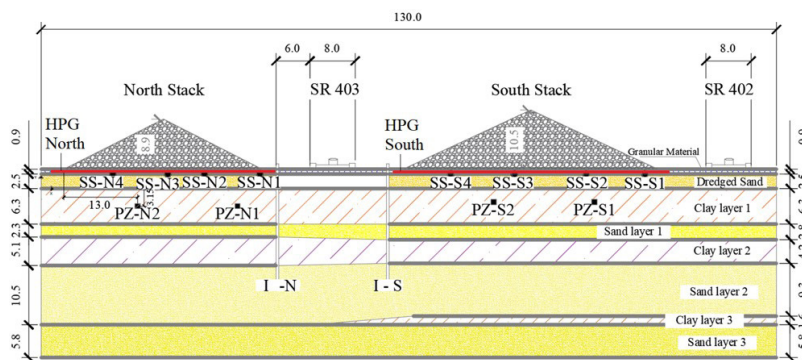


Figure 15. Instrumentation positions in the studied section (dimensions in meter) (Lima et al., 2019).

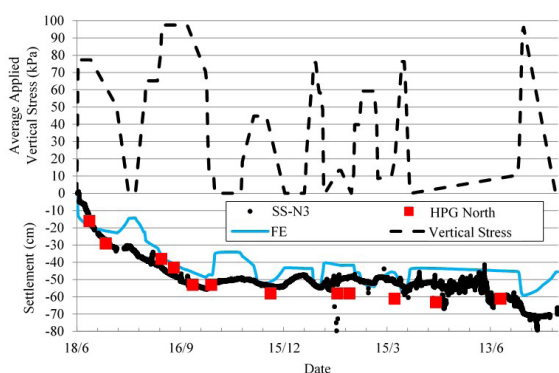


Figure 16. Measured and predicted settlements versus time at northern stack (Lima et al., 2019).

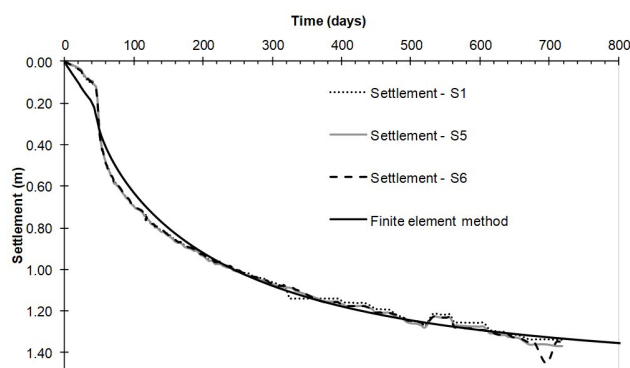


Figure 17. Comparison between measured settlements and predictions from finite element analysis (Riccio Filho et al., 2022).

4.2.3 Sewage plant test embankment

An embankment at a sewage treatment plant, located in the city of São Gonçalo, state of Rio de Janeiro, was supported by *VSCs* with a low area replacement ratio, equal to 7.5% ($d_c = 0.90 \text{ m}$ $s = 2.90 \text{ m}$). Riccio Filho et al. (2022) presented results of monitoring and numerical studies of a 5.35 m high test embankment built on a mesh of ten-by-ten stone columns (*VSC*) built at the site. Analytical and axisymmetric unit cell finite element analyses were compared to the instrumentation data. The measured settlement-time curves were compatible with finite element analysis and favorable regarding settlement values and improvement factors, using the Priebe (1995) method. The low area replacement ratio used was quite effective in reducing the time for settlement stabilization and in providing adequate short-term stability against failure. The improvement factor (β) was equal to 1.43, when comparing the calculated settlement without treatment (2.05 m) to long term settlements after treatment with *VSCs* (1.43 m). Comparison of measured settlements and predictions from finite element analysis is shown in Figure 17. The settlements were measured with three settlement plates (*S1*, *S5* and *S6*) placed over the top of the columns.

Limit equilibrium stability analyses for the end of construction condition were performed for the conditions

of treated and untreated clay foundations. The hypotheses regarding the foundation strength and the computed values of the factors of safety (Morgenstern-Price method) are presented in Table 2. The results show that the *VSC* treatment was quite effective in satisfying the ultimate limit state condition for which the standard requirement is a factor of safety greater than 1.5.

4.3 Final remarks

Vibro-Replacement with Stone Columns are commonly recommended for soft clay deposits with undrained strength values greater than 15 kPa. However, the soft clays sites studied here, with a typical value of undrained strength S_u around 10 kPa, showed quite good performance overall. Considering the limited number of studies of the application of *VSC* in soft soils with undrained strength values around 10 kPa, these studies showed that finite element calculations may be a satisfactory design tool to complement analytical methods.

5. Granular encased columns (*GEC*)

Granular columns have been one of the most effective methods to improve load-bearing capacity, reduce deformations,

and hasten consolidation of soft soil supporting embankments. When extremely soft soil exists, the lateral stress provided by the soft soil is not sufficient enough to prevent excessive bulging that may cause the granular columns tend to fail even under low embankment loading (Almeida et al., 2018b).

In such cases, using geosynthetic encasement could provide additional hoop stress to the granular columns, magnifying the load-capacity and reducing total deformations of the subsoil. In addition, the encasement acts as a barrier which prevents the aggregates clogging thus maintaining the radial drainage capacity of the granular columns. Raithel & Kempfert (2000) developed a widely used design method to calculate embankments on geosynthetic-encased column (GEC).

5.1 Test embankment

Despite of the available investigations on the performance of the GEC, there are limited studies where the field behavior

of GEC-supporting embankment was reported. This section aims to provide further explorations on the behavior of embankment over GECs using measurements provided by instrumentations.

The test embankment was performed in the stockyard of Ternium Company located at Itaguaí, State of Rio de Janeiro. An extensive site investigation was carried out aiming to define the geotechnical properties of the layered subsoil, as shown in Figure 18. Accordingly, the soil profile was characterized by 10 m-thick soft clay improved by 36 GECs installed in a square pattern. The GECs were 11 m in length, 0.8 m in diameter, and installed in center-to-center spacing of 2.0 m producing an area replacement ratio a_c equal to 12.5%. The encasement material was woven geotextile with a tensile stiffness and allowable tensile strength of 1750 kN/m and 95 kN/m, respectively.

Figure 19 illustrates the embankment center line section with the position of the instrumentation as follows:

Table 2. Limit equilibrium stability analyses for the end of construction condition (Riccio Filho et al., 2022, adapted).

Condition	Hypothesis regarding the foundation strength	Factor of safety
untreated clay foundation	corrected S_u (Bjerrum, 1973)	0.90
treated clay	column-clay composite foundation concept (Priebe, 1995)	2.27

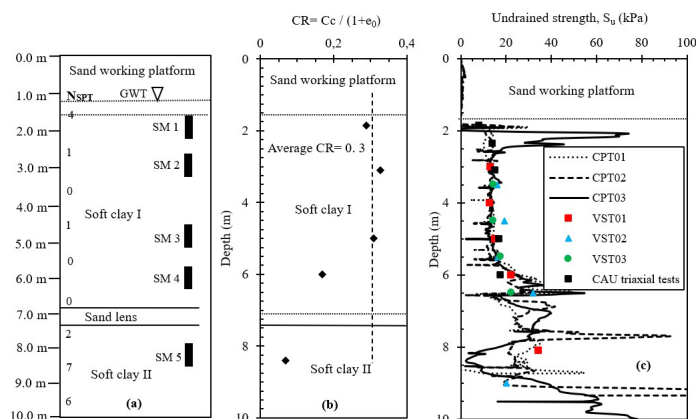


Figure 18. Geotechnical properties of soft clay layers: (a) typical soil profile, (b) compressibility ratio (CR), (c) profile of undrained shear strength (Almeida et al., 2015).

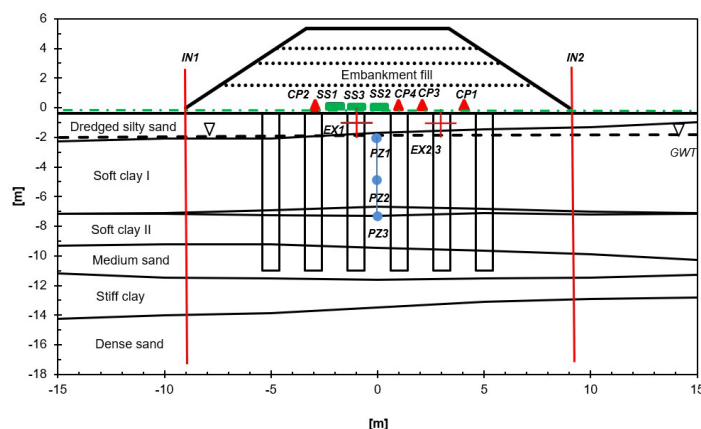


Figure 19. Embankment side view and position of instruments (Almeida et al., 2015).

- Three vibrating wire settlement sensors to measure settlement on top of the soft soil (*SS1*; *SS2*) and on top of the *GEC* (*SS3*);
- Three vibrating wire piezometers installed in soft soil at the depths of: 3 m (*PZ1*), 6 m (*PZ2*) and 8 m (*PZ3*), placed in the embankment centerline;
- Four total stress cells to measure the vertical stresses on the soft soil (*CP1*; *CP3*) and on the *GEC* (*CP2*; *CP4*);
- Three extensometers (*EX*) attached to the geotextile encasement to measure the geotextile hoop strain;
- Two inclinometers (*IN*) to measure distribution of lateral deformation of the soil beneath the embankment toe.

The fill was constructed using sinter feed materials placed in four layers including the consolidation intervals with the total height of 5.35 m. The fill materials had a total unit weight of about 28 kN/m³ thus equivalent to 150 kPa total vertical stress. The embankment was then left in place for 180 days while the measurements were continuously recorded.

5.2 Settlements and improvement factor

Figure 20 shows central plates settlements data on *GEC* and surrounding soil. Measurements are also compared with those predicted by finite element analyses using the axisymmetric unit cell approach. The soft soil and granular materials were modeled by Cam-clay and Mohr-Coulomb criteria, respectively. A good agreement is seen between measurement and numerical analysis which is also obtained for pore pressures in the clay and vertical stresses on the *GEC* and in between columns as presented by Hosseinpour et al. (2015).

The settlement improvement factor (β), defined by the ratio of the settlement for un-improved to that for the *GEC*s-improved ground, is compared with that available from the literature, as shown in Figure 21. The largest measured settlement shown in Figure 20 was used to compute the settlement reduction factor $\beta = 2.8$ for the present field study ($a_c = 12.5\%$ and $J = 1750$ kN/m), which, as seen in Figure 21 (open red circle), suitably falls within the range reported by the literature. The reference settlement in soil was 490mm for calculation of β . Figure 21 also shows the data of other two Brazilian test sites (Riccio Filho et al, 2022; Sandroni, 2014) on stone column without encasing ($J = 0$) mentioned in section 4. It is observed that these two case histories (blue and green circles) are within the overall range of *VSC* data ($J = 0$).

5.3 Stress concentration factor

Figure 22a shows vertical stress measured over the *GEC* and in between aligned columns. The stress concentration factor (n), defined as total vertical stress supported by *GEC* to that measured on surrounding soil, was also assessed.

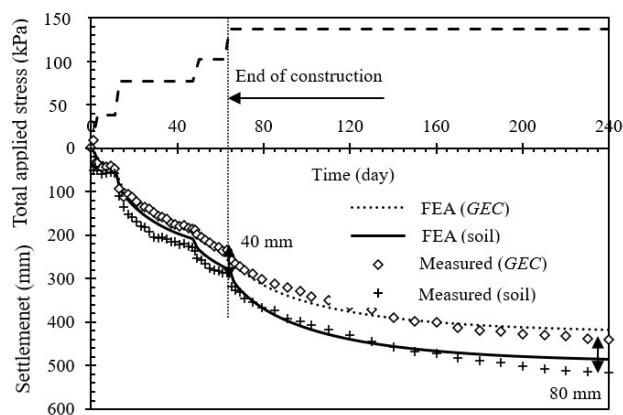


Figure 20. Variation of settlement over the encased column and soft soil (Hosseinpour et al., 2015).

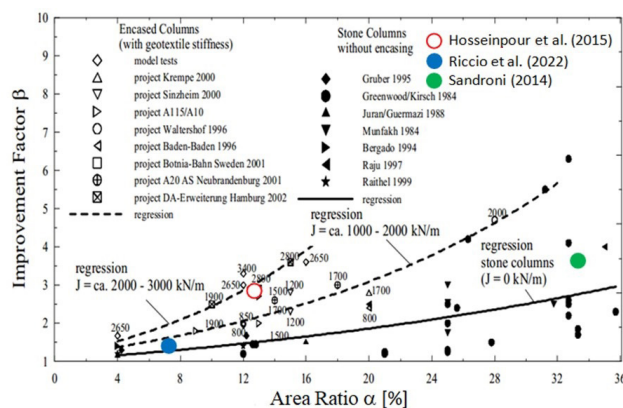


Figure 21. Settlement improvement factor for present test embankment compared with previous case histories (adapted from Almeida et al., 2018b).

Almeida et al. (2013) showed that the stress concentration ranges between 2 and 3 for un-encased columns, but in cases without a working platform “ n ” can be as high as 10 for *GEC*. The low measured value of $n = 2.3$ might be attributed to the existence of a thick sand platform which may modify the stress distribution. The evolution of stress concentration factor shows that there is a reduction in the stress on soil due increase of stiffness in the soil. This increase is due the consolidation along time.

5.4 Effectiveness of *GEC*s

In order to verify the effectiveness of *GEC*s, the maximum settlement under the present test embankment (*GECI*) is compared with that measured for a reinforced test embankment (*REI*) on a soft clay with quite similar geometrical and geotechnical properties (Magnani et al., 2010).

5.4.1 Settlements

Figure 23 represents embankment settlement against corresponding total applied load for both *GECI* and *REI*.

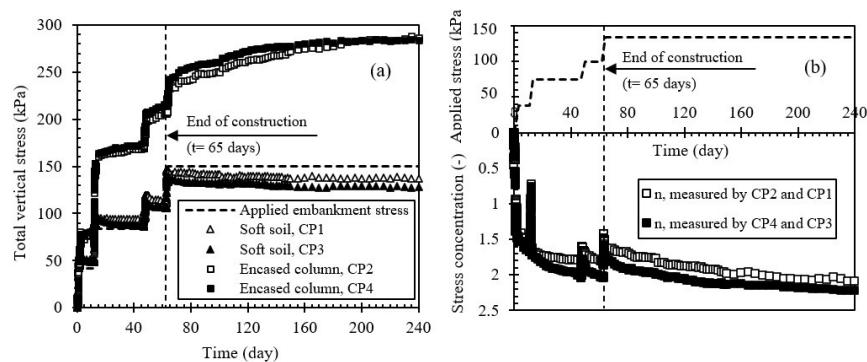


Figure 22. Measurements by stress cells: (a) total vertical stress, (b) stress concentration factor (Hosseinpour et al., 2015).

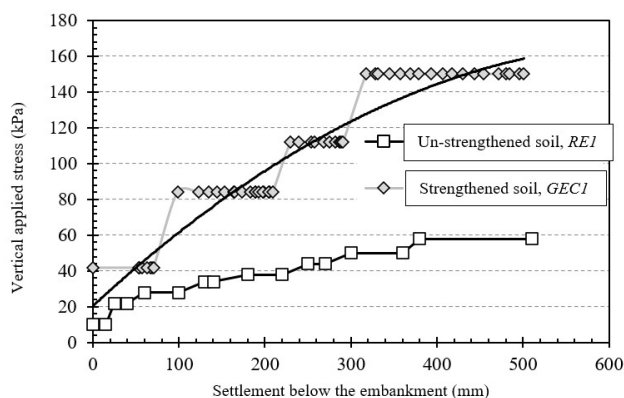


Figure 23. Maximum settlement vs. vertical applied stress for reinforced embankment (*REI*, Magnani et al., 2010) and improved (*GECI*, Hosseinpour et al., 2016) foundations.

It is observed that the *GECs* cause a substantial reduction on the settlement. For instance, for a vertical applied stress of 60 kPa the settlement under *REI* is 500 mm; however, this value reduces to about 100 mm for the *GECI*. In addition, when settlement is 300 mm, the *REI* foundation supports a vertical stress of 50 kPa, but *GECI*, instead, supports about 120 kPa.

5.4.2 Horizontal displacements

The effectiveness of *GECs* on soil horizontal displacements is assessed in Figure 24. It is observed that, using *GECs* remarkably reduces the maximum horizontal deformation of the soft foundation. For example, when the total load is 60 kPa, the maximum magnitude for un-improved case (i.e. *REI*) is about 400 mm, over 10 times greater than that measured for *GECI*. Also, *REI* showed a global failure at the vertical load of 60 kPa with a computed safety factor of 1.098. However, the *GECI* did not show any increase in horizontal deformation, while the total applied load was 2.5 times greater than *REI*, with a computed factor of safety of 1.80.

The maximum horizontal deformation can be correlated with the maximum settlement under the embankment (Tavenas et al., 1979). As presented in Figure 25, for the

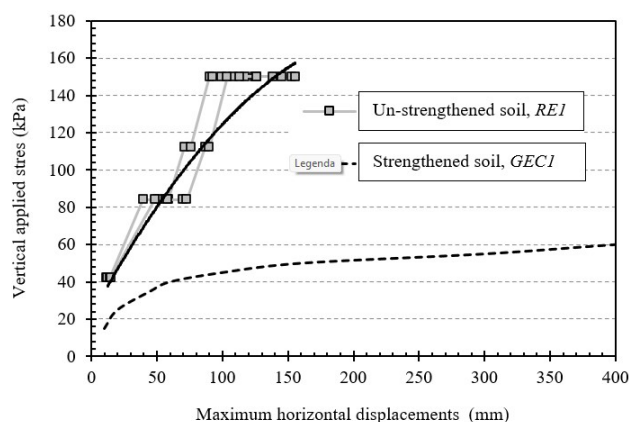


Figure 24. Maximum horizontal displacements vs. vertical applied stress for reinforced embankment (*REI*, Magnani et al., 2010) and improved (*GECI*, Hosseinpour et al., 2016) foundations.

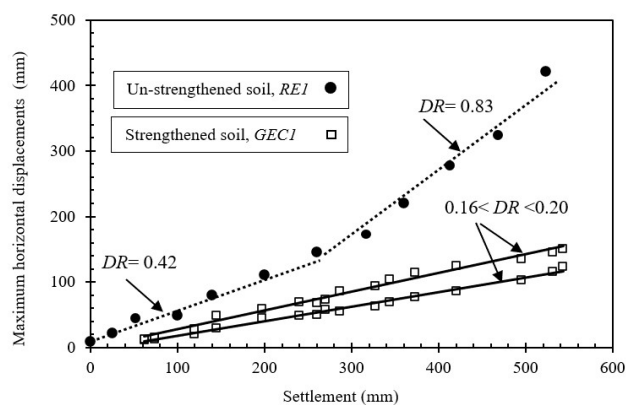


Figure 25. Embankment settlement vs. horizontal displacements for reinforced embankment (*REI*, Magnani et al., 2010) and improved (*GECI*, Hosseinpour et al., 2016) foundations.

GECI the horizontal deformation increased linearly with settlement resulting in a slope (*DR*) ranging from 0.16 to 0.20, much smaller than $DR = 0.42$ for *REI*. Based on measurements, unlike conventional embankments, the use of *GECs* resulted in quite lower values of *DR*, and in the present case, roughly constant during consolidation period.

5.4.3 Excess pore pressure

Figure 26 shows the variation of the excess pore pressure together with the total vertical load for *GECI* and *REI*. For both test embankments the excess pore pressures increased sharply following load application and then dissipated gradually during post-construction. Unlike the *REI*, the maximum excess pore pressure is reduced significantly at *GECI*, while the vertical applied stress was 2.5 times greater than that for *REI*. In fact, the high degree of stress concentration on the top of the *GECs* leads to a reduced vertical stress on the clay. It can also be observed that the radial drainage offered by *GEC* resulted to a faster consolidation for *GECI* and then to a significant improvement in embankment stability during construction.

5.5 Final remarks

From the measurements provided by instrumentation the following outcome can be drawn from the field load test on geosynthetic enclosed columns:

- Measured settlement for the *GEC* and soft soil showed a rapid increase during the 65-day construction period, followed by a more gradual increase during the 6-month consolidation which indicated settlements almost stabilized.
- Compared to a conventional embankment, the embankment on *GECs* with 2.5 times greater vertical stresses showed significantly lower soil vertical and horizontal displacements, and yielded a much larger factor of safety against failure.
- For the *GEC* supported embankment, the ratio of maximum horizontal displacement to maximum settlement varied linearly in the range of 0.16 to 0.2, which was relatively constant throughout the loading and consolidation stages.

6. Piled embankments (*PE*)

Geosynthetic-reinforced piles are commonly used for building structures on soft soils, as this method does not

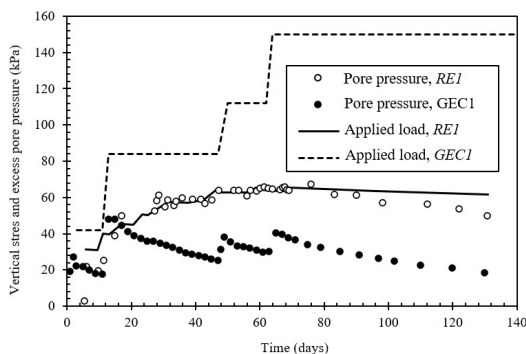


Figure 26. Excess pore pressure and total load vs. time for reinforced embankment (*REI*, Magnani et al., 2010) and improved (*GECI*, Hosseinpour et al., 2016) foundations.

require waiting for the consolidation of the compressible layer. Furthermore, this technique uses lower volume of material than other solutions, resulting in a smaller environmental impact and, in general, fewer maintenance requirements.

This section summarizes the study of a physical centrifuge model, focusing on the geometric parameters covering the typical values used in Brazilian practice (Fagundes et al. 2015, 2017; Almeida, 2019). It is worth mentioning that other preliminary studies, such as Blanc et al. (2013, 2014, 2018), Hartmann et al. (2014), Pinto et al. (2014), Girout et al. (2016) and Almeida et al. (2018a), were very important to the development and conclusions about the behavior of centrifuge models of piled embankments. The centrifuge tests measured the force transferred to the piles, the embankment surface settlements and the maximum geosynthetic reinforcement deflections below the embankment.

6.1 Reinforced piled embankments

The load transfer mechanisms in reinforced piled embankments are shown in Figure 27a. The arching effect (part A) is defined as the load directly transferred to the piles. The remaining total load not transferred by the arching effect is the vertical stress applied to the subsoil and the basal geosynthetic reinforcement (part B + C) (Figure 27b). The geosynthetic reinforcement (*GR*) in tension allows the transference of the remainder of the load back to the piles. This mechanism is called the membrane effect (part B) and its magnitude depends on both the support provided by the soil reaction (part C) and on the *GR* stiffness.

All of these mechanisms are strictly dependent on the area ratio values $\alpha = \pi \cdot d^2 / 4s^2$, where d is the pile diameter, or the cap diameter if there is one, and s is the pile spacing (Figure 27c). The efficiency E is the ability of the embankment to transfer the load F to the piles, as defined by:

$$E = \frac{F}{(\gamma H + q)s^2} \quad (4)$$

The studies presented here focused on a wide range of embankment heights H (1.0 m - 7.2 m), area ratios α in the range of 5% - 20%, two pile diameters, three pile spacing, and two values of tensile stiffness ($J1 = 3.86$ MN/m and $J2 = 16.8$ MN/m), as listed in Table 3.

6.2 Improvement of the load efficiency by reinforcing with geosynthetics

Figure 28 evaluates the influences of the geosynthetic and the *GR* stiffness on load efficiency. Figure 28a shows

Table 3. Centrifuge tests configurations.

Configuration	s (m)	d (m)	α (%)
CF1	2.0	0.5	4.9
CF2	4.0	1.0	4.9
CF3	2.8	1.0	9.8
CF4	2.0	1.0	19.6

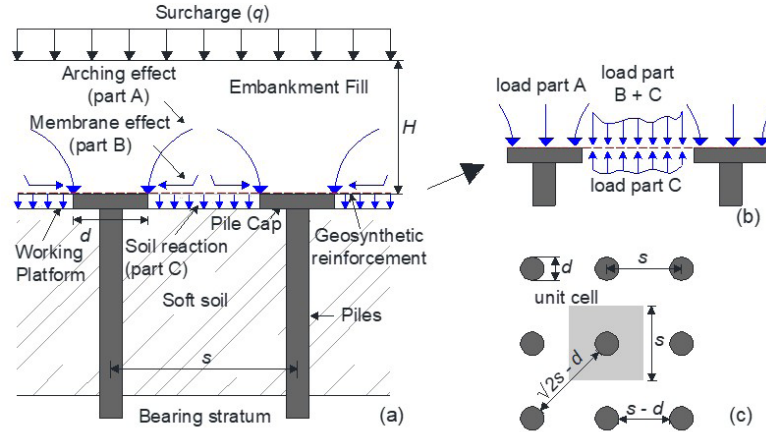


Figure 27. Piled embankments: (a) schematic representation of load transfer mechanisms, (b) distribution of the load parts B and C in the geosynthetic reinforcement, (c) definition of geometric configuration and unit cell (adapted from Fagundes et al., 2017).

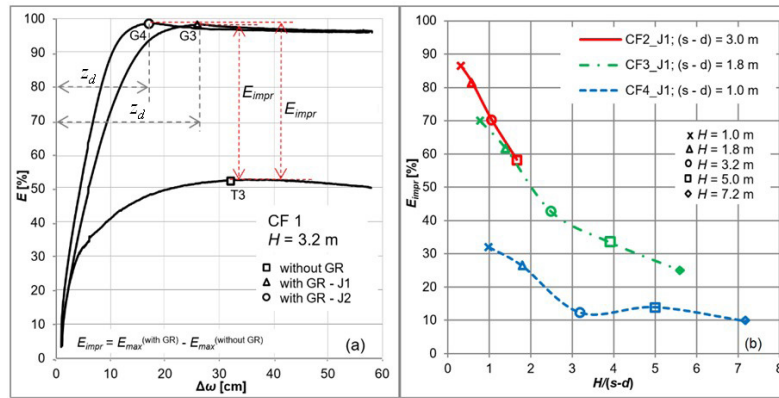


Figure 28. Influence of the geosynthetic in the load efficiency: (a) differences in the load efficiency between tests conducted with and without geosynthetic, (b) efficiency improvement to different test configurations (adapted from Fagundes et al., 2017).

the results of the centrifuge tests with configuration 1 and $H = 3.2$ m, where T3 was performed without GR, and the tests G3 and G4 used the GR J1 and J2, respectively. Figure 28b presents the differences in load efficiency for tests with and without geosynthetic, $E_{impr} = E_{max}^{(with\ GR)} - E_{max}^{(without\ GR)}$. In Figure 28b the E_{impr} is plotted against the embankment height normalized by $(s - d)$ for the configurations with the same diameter d and geosynthetic J1.

In Figure 28a, the value of the load efficiency E increased, reached a peak value, and then reached at a constant value, while the basal embankment settlement $\Delta\omega$ increased continuously. For tests performed with GR, the E_{max} is approximately 100% and the $\Delta\omega$, at which E_{max} was reached, is the main difference between the tests. As E_{max} is reached, the vertical stress applied to the subsoil decreased to zero, i.e., no stress is applied to the soft soil. In other words, the geosynthetic is no longer in contact with the tray and the GR maximum deflection (z_d) has been found, as indicated in Figure 28a. Values of z_d increased with the increasing clear span between the piles $(s - d)$ and the decrease of the GR tensile stiffness. The z_d also increases slightly as H increases.

Results from Fagundes et al. (2015, 2017) are summarized in Figure 28b and show that the geosynthetic reinforcement always improves efficiency. The efficiency improvement E_{impr} is evidently influenced by the clear span $(s - d)$ and the embankment height H (Figure 28b). This improvement in efficiency increases for a larger clear span and a lower embankment height, i.e., when the arching mechanism is less effective: $H < H_{crit}$. For the tests performed with the same configuration, it was observed that the influence of the GR stiffness on the E_{impr} was negligible. However, as mentioned before, E_{max} was reached at lower basal settlements for tests with J2 (Figure 28a).

6.3 Analytical versus experimental results: geosynthetic deflection

The maximum deflection of the geosynthetic (z_d) occurs when the loss of contact between the geosynthetic and the soil below takes place (part C is not present) and this value is achieved with the determination of E_{max} . This loss of contact occurs at the mid-point of the diagonal distance between two

piles z_d (mid center between four piles). However, analytical methods calculate the deflection z longitudinally between piles. Fagundes et al. (2017) and Almeida et al. (2020) suggest adopting $z_d/z = \sqrt{2}$, based on experimental and numerical models. Therefore, the procedure adopted in this study was to first obtain z_d experimentally at E_{max} , thus $z = z_d/\sqrt{2}$, which was then compared with values of z calculated analytically.

Figure 29 presents the comparative values of z , inferred experimentally, with analytical predictions of z using the two analytical methods: BS 8006 (BS, 2012) – Figure 29a and EBGEO (2011) – Figure 29b. A hashed trend line is included in Figure 29 and the agreement between the analytical methods and experimental values are quite good for BS 8006 (BS, 2012) and EBGEO (2011), but less satisfactory for CUR (2016). The BS 8006 (BS, 2012) guideline (Figure 29a) provides the best agreement with an under-prediction of around 1%, while EBGEO (2011) over-predicts experimental values by about 7%, on average (Figure 29b).

6.4 Experimental versus numerical results: differential settlement

The settlements at the embankment base and embankment surface are key factors in understanding the behavior of

piled embankments. Figure 30 presents photographs of the embankment surface at the end of the tests without differential settlement (Figure 30a) and for a test of a low embankment where differential settlements were observed (Figure 30b). Figure 30c shows the differential settlement normalized by the basal embankment settlement ($\Delta u/\Delta \omega$) versus the normalized height of embankment by the clear span $H/(s-d)$ for all pile configurations evaluated. The trend lines passing through the data points intercept the line of $(\Delta u/\Delta \omega) = 0$, which indicates the values of $H/(s-d)$ (Figure 30c) corresponding to the critical height for each geometric configuration evaluated.

The commonly required serviceability state condition is zero differential surface settlement. It is important to point out that, in practice, the major problems related to the differential settlements are in the post-construction phase, however, part of the differential settlements also occur during the construction phase. Based on the results of this paper, to ensure that no differential settlement occurs on the embankment surface, a value of $H/(s-d)$ greater than 2.1 is necessary, but this value depends on α (Figure 30c).

3D numerical modelling results (Almeida, 2019) were compared with experimental data (Fagundes et al., 2017), in order to validate the numerical model (Figure 31a). The vertical displacements in the numerical models with

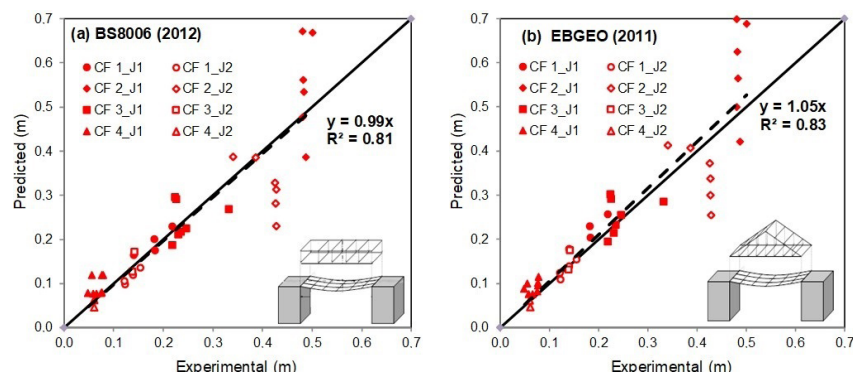


Figure 29. Comparison between the maximum deflection z_d observed experimentally (from E_{max}) and predicted by analytical methods: (a) BS006 (2012) and (b) EBGEO (2011) (adapted from Almeida, 2019).

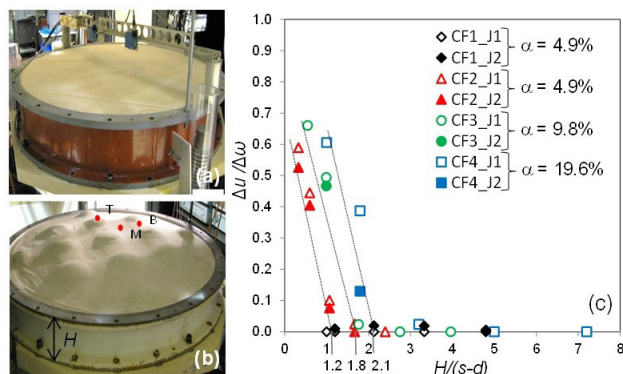


Figure 30. (a) and (b) Surface view of the embankment and (c) the $(\Delta u/\Delta \omega)$ vs $H/(s-d)$ for all configurations (adapted from Fagundes et al., 2015, 2017).

a CF3 configuration and different embankment heights are shown in Figure 31b, c and d.

The results obtained through numerical analyses and experimental results indicate that the differential settlement at the top of the embankment increases to a maximum point, followed by a constant value. The computed values of the differential settlements remain constant because the geosynthetic, after reaching its maximum deflection, sustains the entire embankment load, but the mobile plateau continues to move. A good agreement is generally seen between the experimental and numerical results.

The numerical and experimental results indicated that surface differential settlement decreased with an increase in embankment height and an increase in area ratio (or decrease in pile spacing). Thicker embankments showed negligible surface differential settlement Δu . The surface differential settlements were more dependent on the relationship between the clear span and the embankment height than on the presence of the *GR*. The stiffness of the reinforcement reduced the magnitude of Δu but did not affect the critical height (H_{crit}). The stiffer reinforcement *J2* leads to a greater reduction in Δu than in *J1*.

6.5 Analytical versus numerical results: tensile forces

3D numerical modeling (Almeida, 2019) was performed to compute the geosynthetic tensile forces not measured

in the physical models, compared with values predicted by the European design guidelines. Figure 32 compares the maximum tension of the geosynthetic reinforcement obtained from both numerical and analytical methods. The geosynthetic was simulated with a linear elastic constitutive model. The anisotropic behavior of the *J1* geosynthetic was modeled using the values of $J_x = 4760$ kN/m (Figure 32a) and $J_y = 2960$ kN/m (Figure 32a) for the secant stiffness for directions x and y, respectively.

Figure 32 shows both the numerical and analytical values, indicating that, as expected, the maximum tensile forces T_{max} increase with increasing embankment height and decrease with the reduction in the clear span between piles. Analysis of the results of T_{max} for the three analytical methods shows that the BS 8006 (BS, 2012) values of T_{max} are higher than those obtained with EBGE0 (2011); both of these yielded higher values than those obtained for both load hypotheses assumed in CUR 226 (CUR, 2016).

Comparison between numerical and analytical calculations show that for CF3 (Figure 32a and b), the values of T_{max} computed with EBGE0 (2011) and BS 8006 (BS, 2012) are fairly close to the numerical results, although the EBGE0 (2011) values are in better agreement. For the CF3 configuration, the CUR226 (2016)-uniform provides reasonable agreement where $H = 1.0$ and 5.0 m, but only for J_y (Figure 32b).

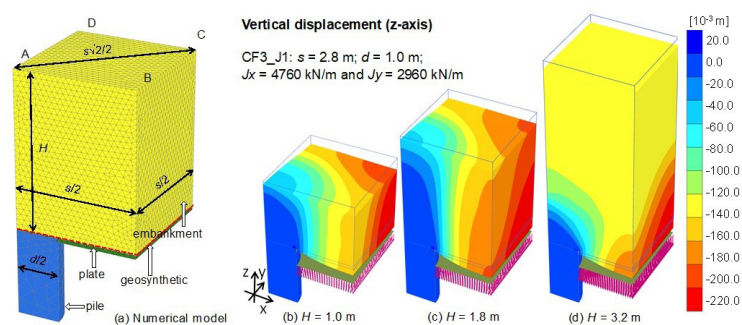


Figure 31. 3D View of the numerical model; vertical displacements to a CF3_J1 and different embankment heights.

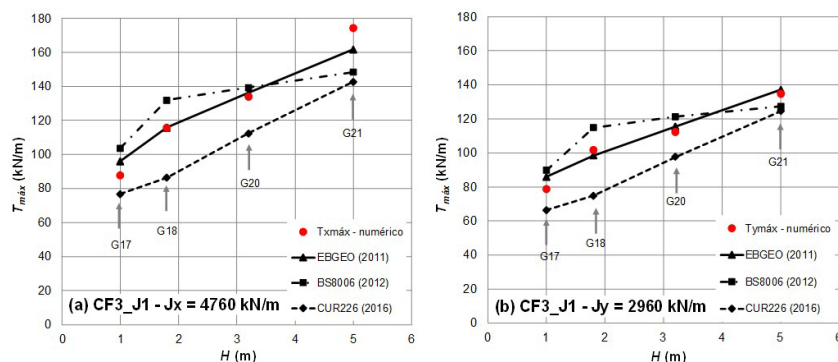


Figure 32. Maximum tensile force of the geosynthetic as a function of the embankment height obtained with the numerical models and the analytical method: a) $J_x = 4760$ kN/m; b) $J_y = 2960$ kN/m (adapted from Almeida, 2019).

6.6 Final remarks

The studies on piled embankments (*PE*) showed that the membrane effect, combined with soil arching, provides values of efficiency (regarding load transfer to the piles) close to 100% for most tests. The efficiency is influenced more by the height and clear span between piles than by the stiffness of *GR*. To ensure that no differential settlement occurs on the embankment surface, a value of $H/(s-d)$ greater than 2.1 is recommended.

The EBGeo (2011) and BS (2012) guidelines for *PE* yielded good results in the assessment of measured versus computed geosynthetic deflections in the centrifuge tests. Numerical results showed that the maximum tensile forces, with arching and membrane effects in full operation, occur at the pile edge and increase with embankment height, surface surcharge and geosynthetic stiffness.

7. Deep soil mixing (DSM)

7.1 Principles and applications

The Deep Soil Mixing (*DSM*) technique was developed in the United States in 1954, but the methodologies most often used today are based on techniques used in Japan and Scandinavian countries (FHWA, 2013). According to Topolnicki (2016), the first application of the *DSM* technique in Scandinavia occurred in the 1960s using quicklime as binder. The effectiveness of using lime was confirmed in the studies performed in the '70s and in more recent studies conducted in Japan. The cast-in-place columns are built by mixing the soft soil with a binder. According to Kitazume & Terashi (2013), soil mixing can be done by adding lime, cement or a combination of these two binders with other special ones. *DSM* application and the related dosage of soil-binder mixtures are guided by EN 14679-2005 (EN, 2005).

DSM uses cast-in-place columns with diameters typically varying from 0.40 m to 2.40 m for a single column, according to Topolnicki (2012, 2016). The piled embankment technique described in section 6 uses piles which are generally driven. The Deep Soil Mixing (*DSM*) technique, shown in Figure 33 for piled embankment, uses cast-in-place piles.

The vertical axial stress (σ_v) acting on the top of the column can be calculated by the piled embankment methods presented in CUR226 (2016), EBGeo (2011) and BS 8006 (BS, 2017). While the German recommendation (EBGeo, 2011) is based on Kempfert et al. (2004), the Dutch standard (CUR226, 2016) is based on van Eekelen et al. (2013). However, in general, a system efficiency of 100% is usually assumed for a robust design of piled embankments.

Once the σ_v is determined, the binder content needs to be calculated in order to achieve the required unconfined compressive strength (q_u) to support the σ_v . According to Topolnicki (2016), the secant elastic modulus ($E_{50\%}$) can be

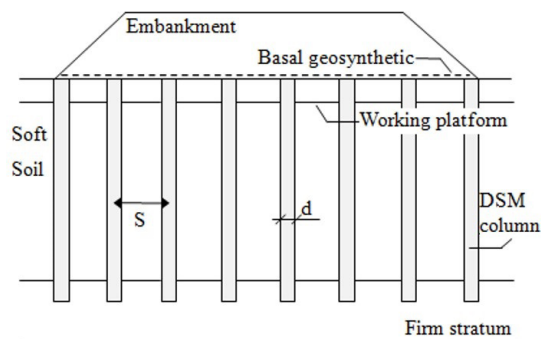


Figure 33. Typical use of *DSM* columns with diameter d for piled embankment on soft soils, piles spaced s center to center.

estimated, as a first approach, from Equation 5 based on the value of q_u . The value of $E_{50\%}$ enables the evaluation of the elastic settlement of the embankment.

$$E_{50\%} = 380 \cdot q_u \quad (5)$$

The q_u value is obtained from the statistical analysis of a series of unconfined compressive strength laboratory tests performed 7, 14, 28 and 56 days after installation of the *DSM* column.

The design parameter $f_{ck,28}$ is related to the 90% confidence interval of 90% for all values of q_u . According to the Topolnicki (2016) the *COV* value must be equal to or less than 0.38 for *DSM* applications in cohesive soils and the S_d (standard deviation) must be determined.

One of the most important factors in the design of an embankment supported by *DSM* columns is the analysis of the critical height (H_{crit}). If the height of the embankment is not greater than this value, the spacing between columns must be reduced. The H_{crit} is defined by McGuire et al. (2012) according to Equation 6.

$$H_{crit} = 1.15s' + 1.44d \quad (6)$$

where: s' is a geometric parameter, S is the space between axes and d is the diameter of the column. For a square mesh pattern, the most common one, Equation 7 should be used.

$$s' = \frac{\sqrt{2} \cdot S^2}{2} - \frac{d}{2} \quad (7)$$

Alternatively, the H_{crit} can be calculated according to EBGeo (2011), which also accounts for live loads. Another very important parameter is the replacement ratio (α), which provides the ratio between the area of a column and its area of influence given by Equation 2 in section 4. Typically, α ranges from 0.10 to 0.20 for *DSM* applications in piled embankments.

In the next section two case studies using *DSM* applications are presented. Both cases are located at the

Salgado Filho International Airport, Porto Alegre, Brazil. The first case is the cargo terminal and the second is the extension of the takeoff and landing runway.

7.2 DSM at airport cargo terminal

The air cargo terminal, in Salgado Filho international Airport and was built in 2014. The soil profile in the region of the cargo terminal, in general, is composed of three main soil layers: a pre-existing upper embankment (0.0m to -2.0m), a soft clay soil layer (-2.0m to -10.0m) and below it, residual soil.

Table 4 shows the main characteristics of the soft clay used in the design of the DSM columns. Note that the organic matter content (*OMC*) is less than the maximum acceptable value of 15% and the *pH* of 5.5 indicates low aggressiveness of the soil.

Unconfined compressive strength tests were performed to obtain the optimum content of binder (cement CII-Z-32, lime, cement and lime, etc) in the mixture. The tests were carried out with seven soil-cement mixtures, which results are shown in Figure 34.

Figure 34 shows that the greatest increase in q_u occurs between 7 and 28 days, for soil-cement and soil-cement-lime, after which the increase is less pronounced. However, the sand mixture exhibited a linear increase in q_u . A comparison of mixture 4 with mixture 5 and mixture 4 with mixture 6 confirms that the addition of lime produces a decrease in q_u . A comparison of mixture 4 with mixture 7 shows that the addition of sand produces an increase in q_u . The behavior observed for mixture 4 was different, with no increase in q_u from 28 to 56 days. In this study, mixture 3 was chosen, presenting unconfined compressive strength at 28 days equal to 1.35MPa based on 130 laboratory tests. In the field, the average q_u value reached a value of 1.78 MPa (greater than 1.35 MPa required in the design) with a confidence interval of 90% and a *COV* equal to 0.31 (within the interval expected for DSM for cohesive soils, Topolnicki, 2016).

The DSM columns used in the project had a diameter of 0.80m, a distance of 2.25m between column axes configured

Table 4. Characteristics of the soft soil in the Salgado Filho airport (Machado, 2016).

Parameter	Parameter
w	94%
w_p	34%
w_L	69%
<i>PI</i>	35%
γ_s (gf/cm ³)	2.58
γ (gf/cm ³)	14.8
<i>OMC</i>	8.80
<i>pH</i>	5.50

Note: w = soil natural moisture; w_p = plasticity limit; w_L = liquid limit; *PI* = plasticity index; γ_s = unit weight of solids; γ = unit weight; *OMC* = Organic matter content; *pH* = potential of hydrogen.

in a square mesh pattern (area ratio $\alpha = 9.90\%$), an average length equal to 6.50 m with a 1.00 m penetration in the residual soil layer below. Figure 35 compares field measurements, taken at Test Area 2, located adjacent to the Cargo Terminal, with axisymmetric finite element predictions using PLAXIS 2D software. In Figure 35, “field measurement” represents the average measured settlement from three settlement plates (*PR01*, *PR03* and *PR11*). The beginning of embankment construction has occurred after 28 days and the reduction of settlements was pronounced.

7.3 DSM at extension of the takeoff and landing airport runway

The study reported in this section is related to the extension of the takeoff and landing runway (approx. 1.00 km) was built in 2019 at the Salgado Filho International Airport that. The DSM technique was applied in the soft clay ground at the site to support the embankment and pavement. The embankment has a maximum height of 5.50 m reaching 6.50 m with applied surcharge. A square mesh pattern was

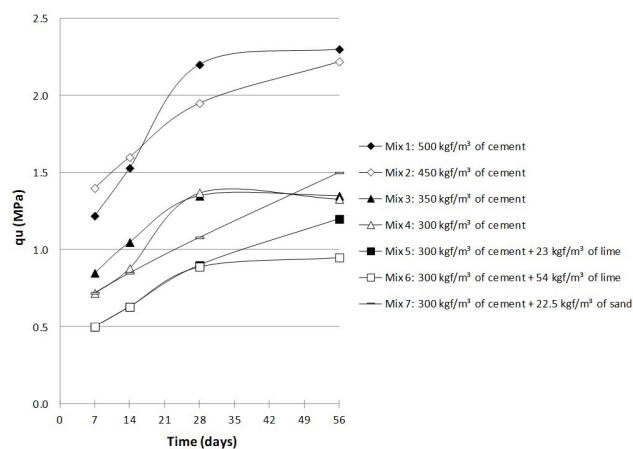


Figure 34. Increase in the q_u with time (days) for mixtures 1-7, adapted from Machado (2016).

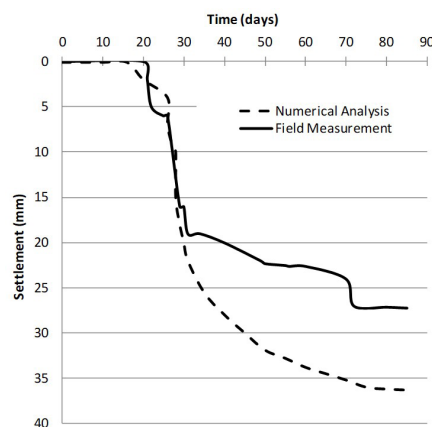


Figure 35. Comparison between numerical predictions and settlements measured in the field (Test Area 2), adapted from Assis (2016).

used, with a 0.80 m column diameter and a 1.80m distance between column axes (area ratio $\alpha = 15.4\%$). The column length was 9.00m on average and a basal geogrid layer was installed on the top of columns.

Figure 36 presents the evolution of q_u with time. The data in the graph is the average q_u at 7, 14, 28 and 56 days obtained from laboratory tests with samples taken directly from the columns using the wet grab method. In total, specimens taken from 450 DSM columns were tested. The embankment construction starts after 28 days after installation of columns.

According to Figure 36, the q_u required by the project was reached at approximately 10 days. The mixture was prepared with 350 kgf/m³ of cement. Statistical control yielded an S_d value of 0.55 MPa and a COV of 0.33, within the interval expected for the use of DSM for cohesive soils (Topolnicki, 2016).

Displacements were monitored by means of settlement plates, showing good performance in terms of embankment stabilization. Figure 37 shows that the settlements were minimum, reaching a maximum value of 17 mm for the embankment (plus surcharge) height of 6.50 m. In Figure 38, SPOG1 and SPOG2 are the settlement plates over the geogrid and between columns and SPOC is the settlement plate over the geogrid and column top.

The vertical stresses at the top of the column (σ_{vc}) and in between columns (on top of the soil, σ_{vs}) were measured by means of total cells. These measurements enable determination of the stress concentration factor $n = (\sigma_{vc} / \sigma_{vs})$ shown in Figure 27. The value of n over time computed from two sets of total stress cells (A and B) is shown in Figure 38, and as the embankment is heightened, a load transfer from the soil to the column takes place. This load transfer occurs even after the 45-day period of construction of the embankment. It appears that clay consolidation due to work platform loading below the geogrid enhances this load transfer. The built of embankment starts after 28 days of columns installation.

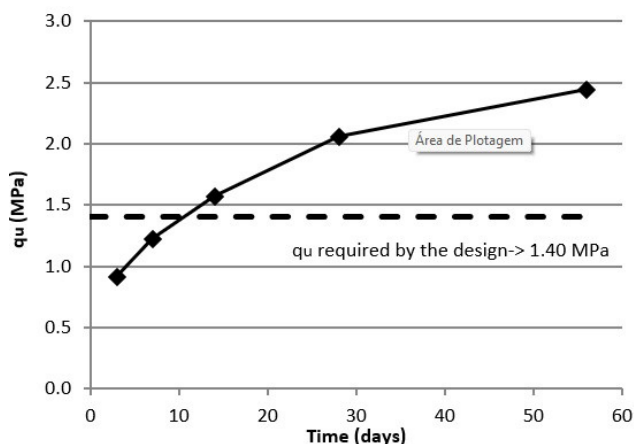


Figure 36. Evolution of q_u with time, field tests (Ávila, 2021).

7.4 Final remarks

For the two case histories reported here (Airport Cargo Terminal and Runway), the DSM application showed very small settlements, of the order of a few centimeters, and overall good performance. The resulting stress concentration factor (n) indicated that part of vertical stresses imposed by the embankment transferred to the columns, significantly reducing the settlements, which were minimum. Therefore, the use of DSM columns permitted rapid construction of the embankments, meeting the requirements of the construction schedule.

The practice experience in Brazil with soft soil improvement using SSM with Portland cement permitted the following conclusions:

- The technique is efficient for very soft soils ($N_{SPT} < 2$), with high moisture content;
- Significant settlement occurs within a short period after each load step, and a large portion of the total settlement occurs within the preloading period;

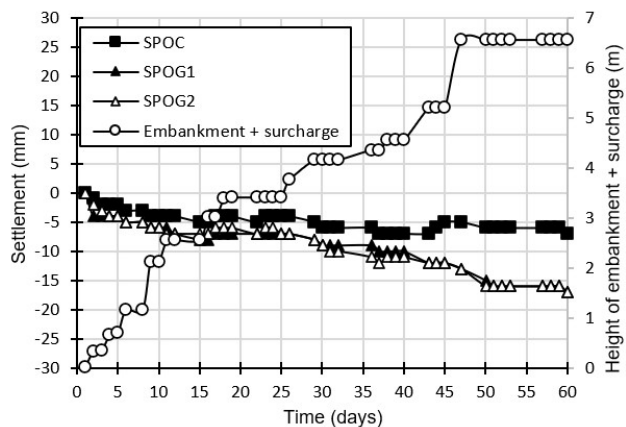


Figure 37. Evolution of the settlements, column top (SPOC) and between columns (SPOG1 and SPOG2) over the time, adapted from Ávila (2021).

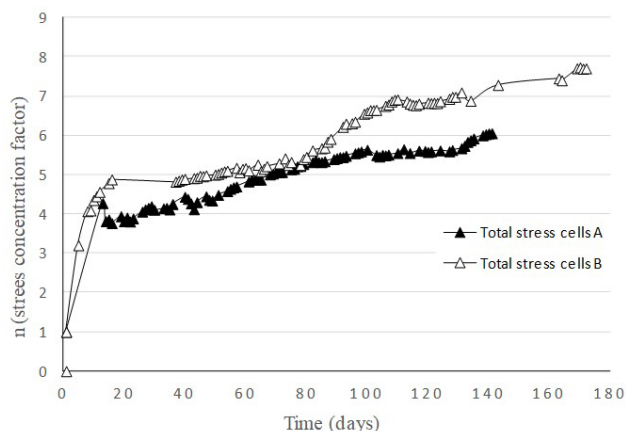


Figure 38. Evolution of the n over time (Ávila, 2021).

- Significantly reduced values of field strength and stiffness compared to the laboratory tests was possibly caused by the difficulty of field homogenization;
- The stabilized soil is shown to be a heterogeneous soil mass, with variable characteristics, mainly influenced by difficult field mixing and variable cement content in different portions in the mass.

8. Shallow soil mixing (SSM)

Shallow soil mixing (SSM) emerged in the 1990s, as a suitable and economically viable method for the stabilization of soft soils (Massarsch & Topolnicki, 2005). In Brazil, the technique has been used for about 15 years, with the commercial name of STABTEC® (Andrade et al., 2010). The technique consists of mechanically mixing a powder binder into soft submerged soils. The equipment available in Brazil has a maximum depth limitation of 6.0 m, but there are reports of equipment reaching up to 8.0 m (Forsman et al., 2015). The technique has the advantage of minimal waste generation, reducing material transport and disposal costs.

8.1 Execution process and main factors involved

The equipment used is an excavator with a hydraulic arm coupled to a mixing tool, connected to feeder tanks. The pressure feeder injects the dry binder powder into the soil directly with the mixing tool, and at the same time, the binder is mixed into the soil. The mixing speed is adjustable and the pressure and dosage of the binder to be injected can be controlled. The area to be treated is divided into cells, with dimensions based on the equipment capacity and the volume of treated soil estimated for the project. Immediately after the mixing, a geotextile is positioned over the stabilized cell and a preloading fill of 1.0 to 1.5 m is applied. The typical equipment and process is illustrated in Figure 39. The purpose of the preloading is to compress the newly stabilized soil mass, forcing the air bubbles formed during mixing to escape, causing immediate settlements, and increasing the strength of the treated mass. The next stage advances over the treated cell on the following day. The main factors involved are the following:

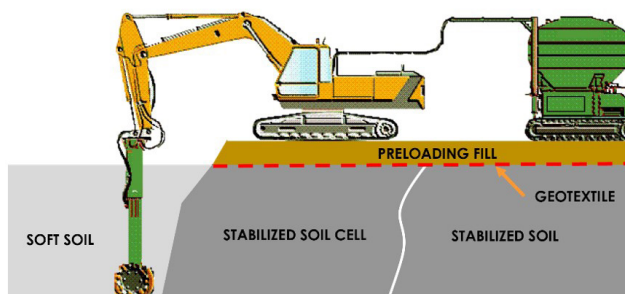


Figure 39. SSM technology (Adapted from Andrade et al., 2010).

- Soil characteristics: In general, SSM is described as applicable to soft surface soil. Brazilian experience has shown that the technique is efficient for very soft soils, with high moisture content and SPT blow count (N_{spt}) less than 2. Generally, for soft soils with higher resistance, the mixing usually becomes inefficient, and homogenization is impaired. Practice experience has also shown that soft soil with sand lens layers, mixed prior to injection of the binder, tend to yield a proportionally higher final strength, due to the increase of sand content in the mass;
- Binders: The most commonly used binders are cement and lime. Binders from industrial processes such as slag, flue gas desulphurization, fly ash and ground glass have also been used, generally combined with cement or lime. In Brazil, high early strength cement is preferred, as it reduces the waiting time to advance to the next step;
- Homogenization: an initial mixing of the soil mass is recommended to obtain a good homogenization for SSM. Thereafter, the homogenized soil is mixed with the binder. The operator must develop continuous and repetitive vertical and lateral movements of the mixing tool, as uniformly as possible. A homogeneous mixture is essential to optimize binder dosage and to obtain the design strength;
- Curing time: the curing time varies with the binder and soil type to be mixed. When using only cement, the stabilization reactions are completed in about a month. When binders such as lime, slag and fly ash are used, the stabilization process can continue for several months (EuroSoilStab, 2002).

8.2 Investigation, design and control

Initially, an analysis of the applicability of SSM should be carried out, considering the site, predicted use, soils characteristics, time available and surrounding conditions. The design comprises the following steps: a) complementary investigations; b) parameter determinations; and c) ultimate limit state (ULS) and serviceability limit state (SLS) verifications, as reported by Almeida & Marques (2013). and EuroSoilStab (2002). In order to define the binder and the dosage, laboratory tests should be carried out on the soil. Soil samples must be collected and mixed in the laboratory with different binders and curing conditions. The bulk unit weight, unconfined compression strength (q_u) and deformation modulus must be determined. The chemical properties of the soil such as pH, chlorides, humic acids, organic matter, ion-exchange capacity, sulfide capacity and total sulphur are important to the strength and durability of the stabilized soil mass and can interfere with the amount and type of binder to be used. If chlorides or organic matter are suspected of contributing to poor stabilization, the pore water should be

extracted from the soil for chemical analysis, as reported by EuroSoilStab (2002).

Laboratory samples have higher strength than the corresponding field stabilized material. The ratio between field and laboratory unconfined compressive strength (q_{uf}/q_{ul}) varies between 0.25 and 0.50 (EuroSoilStab, 2002; Nascimento, 2016). The disparity is attributed to several factors, most notably the homogeneity of the laboratory mixture.

Stability analyses should be carried out, considering the loads and the safety factor, according to the current standards. The settlements during and after the stabilization must be estimated considering the curing time. A temporary surcharge may be considered in order to minimize the residual settlements. The stabilization efficiency can be verified by unconfined compression test (*UCT*) performed in undisturbed samples. Alternatively, Standard Penetration Tests (*SPT*), Cone Penetration Test (*CPT*) and Vane Test could be performed. Embankment settlements and any overloads can be monitored using settlement plates.

8.3 Cases histories

This section presents two studies of the application of *SSM*, related to the execution of embankments for the urbanization of a shopping center area (Centro Metropolitano), in 2015, and a real estate development (Pontal Oceânico), in 2020, both in the city of Rio de Janeiro, Brazil. A summary of the properties of the unstabilized soil from the two sites is presented in Table 5.

Centro Metropolitano: An embankment of 3.0 m was constructed over the soft soil deposit improved with *SSM*. The technique was used due the vicinity of neighboring foundation structures and construction deadline constraints. *SPT* performed locally, Figure 40, indicated the existence of a superficial fill layer of roughly 1.0 m thick over a very soft organic clay with a thickness of 6.50 m, followed by a layer of fine clayey sand. The water level was 0.50 m below the surface.

The specimens were prepared in the laboratory using high early strength cement content relative to the wet mass

of the soil of 100, 150 and 200 kg/m³. As the Service Limit State (*SLS*) was the most relevant factor in this case, the dosage of 150 kg/m³ was chosen (Lemos et al., 2020) based on secant modulus (E_{s0}). The *SSM* in the field was carried out to a depth of 6.0 m. Immediately after the mixing process, a geotextile was positioned over the stabilized cell, and 1.0 m of preloading fill applied. Figure 40 compares site investigation performed before and after ground treatment (curing of 50 days). The *SPT* after *SSM*, showed that the average N_{spt} increased from close to zero for the intact soil to a range of between 2 and 18 for the stabilized soil. The variability of N_{spt} after *SSM* is probably due to the heterogeneity of the

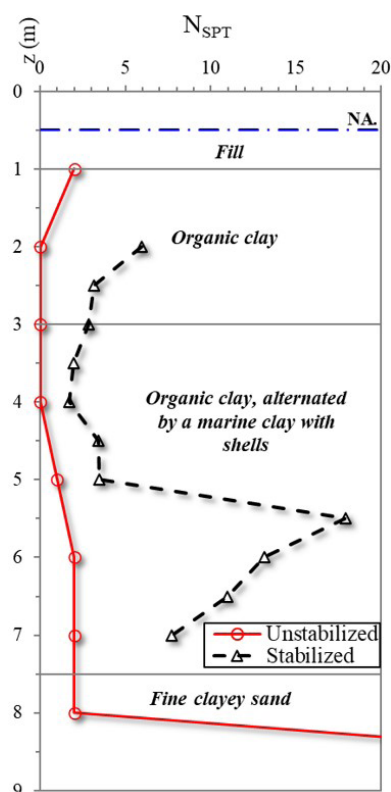


Figure 40. Geotechnical profile of the soft soil deposit: *SPT* for unstabilized and stabilized test results (Adapted from Lemos et al., 2020).

Table 5. Soft soil properties

Properties	Centro Metropolitano		Pontal Oceânico	
	Peat Organic clay		Peat organic clay	Sandy clay
Natural moisture content – w (%)	500-600		525-597	74-87
Liquid limit – w_L (%)	536-540		560-598	53-65
Plastic limit – w_p (%)	200-240		228-246	22-26
Organic matter content – OM (%)	50		65	5-10
pH	3.4		-	-
Specific gravity of soil particles – G_s	1.89		-	-
Bulk unit weight – γ_{nat} (kN/m ³)	10.80		-	-
Clay ≤ 0.002 mm (%)	49		10-20	40-60
Silt > 0.002 mm - 0.063mm (%)	28		-	-
Sand > 0.063 mm - 2.0mm (%)	23		-	-

soil layer, as well as the difficulty of mixing in the field, which resulted in variable cement content in the soil mass. Even so, the settlement control data indicated that the *SSM* results were satisfactory.

Undisturbed samples were collected after 30 days of field curing in order to perform *UCT* to determine the effectiveness of the stabilization. As shown in Figure, the results still exhibited significant dispersion, confirming that the stabilized soil presented variable characteristics, influenced mainly by the cement content of different proportions within the mass. Figure 41 shows that q_{ur}/q_{uL} varied between 0.25 and 0.50. The q_u for the unstabilized soil was 12 kPa average, which is about four times lower than results of the field stabilized soil. Whereas the E_{50} values of laboratory tests were two to three times higher than field values. As pointed out before (EuroSoilStab, 2002; Nascimento, 2016), this commonly observed disparity is associated to the fact that laboratory prepared specimens are more homogeneous than field specimens.

Settlement control was carried out after *SSM* and each embankment step, including a temporary surcharge of 1.50 m height, then maintained for 6 months with negligible settlement values. The total settlement measured in the *SSM* was 0.15-0.30 m significantly lower than the estimate without the *SSM*, of about 1.5 m. The settlement improvement ratio β defined by the value of the final settlement of the soft soil without treatment to the value of the final settlement after treatment, often used in granular columns applications, may be also applied to the present case, was 5 to 10 (França et al., 2016).

Pontal Oceânico: The urbanization of 9,000 m², with a 3.0 m embankment, would cause excessive settlements. The geotechnical investigation included *SPT*, *CPTu* (Figure 42) and unconfined compression laboratory tests. The site presented

a superficial soft soil, 3.0 to 6.0 m thick, composed of peat varying to organic clay, eventually to sandy clay in the lower layer. A second soft sandy clay layer, 2.0 to 4.0 m thick, was also identified an underlying sand layer of 1.0 to 3.0 m thick. The *SSM* with cement binder and temporary surcharge was adopted for the site stabilization and in the specific region with significant thickness of the second soft soil layer, *SSM* was combined with vertical drains.

The unconfined compression tests (*UCTs*) indicated undrained strength less than 10 kPa for the soft soil, with the characteristics summarized in Table 5. For *SSM* validation, *UCTs* were carried out on laboratory mixed samples, utilizing the soft soil with cement content of 120 kg/m³. The tests were divided into mixtures using only peat and using a percentage of peat and sandy clay, non-preloaded or preloaded with an equivalent embankment of 1.0 m height (18 kPa). Different curing procedures were used with no significant differences observed.

Field stabilized undisturbed samples were also collected for *UCT*. The results are presented in Figure 43. The most significant q_u increase occurred with the preloaded samples over the curing period, ranging between 90 kPa in 3 days to 230 kPa in 28 days, on average. No significant q_u increase was observed on the non-preloaded samples for both mixtures. In all cases, including the tests carried out on the field stabilized soil, the strength results were significantly higher than unstabilized soil. The field stabilized soil data shown by red squares in Figure 43 is the relevant data for field conditions.

Field tests and settlement monitoring indicated the importance of applied preloading. The significant initial settlement measured (PR11 and PR202 plates, Figure 44), implies a reduction in the void index in the treated soil,

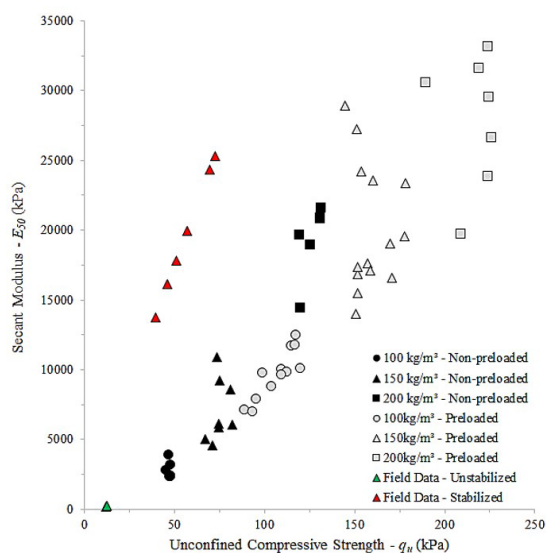


Figure 41. Unconfined compressive strength (q_u) relative to secant modulus (E_{50}) for 18 kPa preloaded and non-preloaded laboratory and field specimens (Adapted from Lemos et al., 2020).

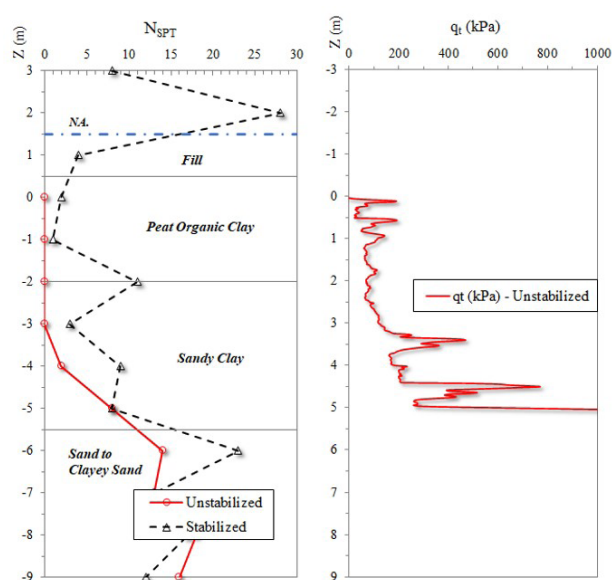


Figure 42. Geotechnical profile of the soft soil deposit, *SPT* and *CPTu* test results.

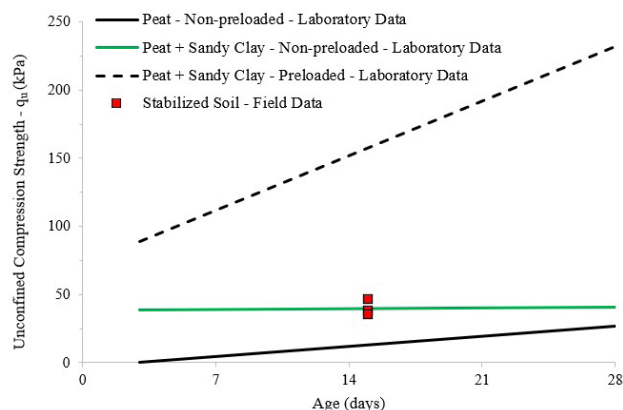


Figure 43. Average results for the unconfined compression strength; non-preloaded and preloaded tests with 18 kPa.

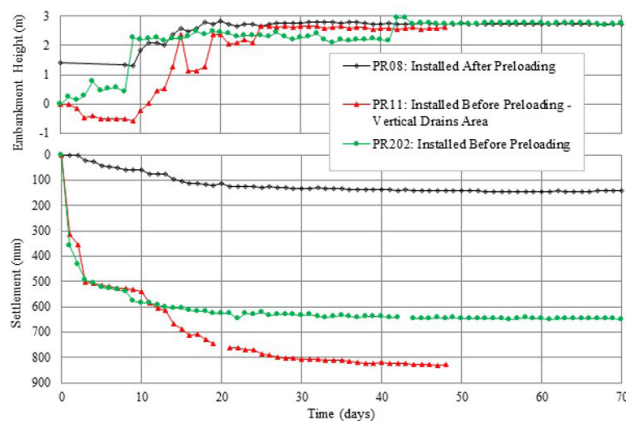


Figure 44. Embankment settlement monitoring.

contributing to a related strength increase. The preloading in lab tests resulted in a significant increase in q_u (Figure 43). On PR08 plate (Figure 44), installed after the preloading period, the resulting deformation was less than 150 mm. On PR202 installed before preloading 80% of the total settlement was measured in the first week, with preloading fill less than 1.5 m high. The same behavior was observed on PR11 installed in a vertical drain area, in which approximately 60% of the total settlement was measured during the preloading period. The total settlement without the *SSM* was estimated in 2.0 m.

8.4 Final remarks

The practice experience in Brazil with soft soil improvement using *SSM* with Portland cement permitted the following conclusions:

- The technique is efficient for very soft soils ($N_{spi} < 2$), with high moisture content;
- Significant settlement occurs within a short period after each load step, and a large portion of the total settlement occurs within the preloading period;

- Significantly reduced values of field strength and stiffness compared to the laboratory tests was possibly caused by the difficulty of field homogenization;
- The stabilized soil is shown to be a heterogeneous soil mass, with variable characteristics, mainly influenced by difficult field mixing and variable cement content in different portions in the mass.

9. CPR grouting

9.1 Introduction

CPR grouting is a technique to improve the strength and deformation characteristics of soft clay soils. It was introduced in Brazil as a variation of compaction grouting in the 2000s. Since then, it has become a time tested and proven technique for soft clay improvement, particularly in remedial situations. *CPR* is the Portuguese acronym ‘Deep Radial Consolidation’.

CPR grouting involves the injection of a low-slump mortar grout into a pre-installed array of prefabricated vertical drains (*PVDs*). This technique appears to have been first proposed by Wu (2005). The philosophy behind the use of artificial drains is to ensure good drainage of fine-graded soils, allowing faster dissipation of the excess pore pressures induced by grouting.

For *CPR* grouting to be effective, the grout should not travel far from its injection point, nor fracture the soil. It must form an “expanding bulb” to displace and radially compress the soil without claquage. Fracturing can occur in clays in undrained conditions if the grout is too liquid. For this reason, a high viscosity grout with high solid content is essential to prevent undesired fracturing (Au et al., 2003).

9.2 Design aspects

The design of *CPR* grouting is based on the modeling framework developed by Cirone (2016). In general, a grouting project includes:

- Installation of vertical drains;
- Grout hole locations, geometry, spacing, maximum depth and inclination;
- Grout mix and properties;
- Refusal criteria;
- The program of work in stages, the drilling technique and the grout stages (top-down or bottom-up);
- Geotechnical testing program for verification of grouting effectiveness (acceptance criteria).

The stages of *CPR* grouting are summarized here. Drains are installed in a triangular or square pattern, with spacing that varies from 1.0 m to 2.5 m. Next, grout holes are intercalated between the drains. A low-slump (max. 10 cm) soil-cement harsh mortar is injected at low pressures of 5-15 kg/cm² through a four-inch open-ended pipe. Grouting

can proceed according to top-down or bottom-up procedures, depending on specific project needs. The grout is injected holding the pipe in place. On reaching either of the refusal criteria, the pipe is raised (or driven) to the next stage, and the process repeated. Common refusal criteria are:

- A maximum grout take (target volume) is attained, as predetermined by the volume replacement ratio.
- Pressure, as measured at the header, reaches a preset maximum operating value.
- Undesired ground or structural movements are detected.

After completion of primary points, secondary and tertiary points are grouted in sequence.

Typical arrangements are shown in Figure 45. For each layout, the unit cell can be defined as the influence zone of each grout hole. The unit cell can be idealized as a cylinder with a cross sectional area equal to the area enclosed by the *PVDs* in the neighborhood.

The degree of improvement is generally calculated on the assumption that the expansion of the bulbs produces a volume change in the ground due to soil consolidation. It can be estimated according the observations reported by Komiya et al. (2001), Au et al. (2007) and Andrade et al. (2022). Bearing capacity and final settlement of the treated soil are calculated with the equivalent homogeneous medium method. This approach adopts equivalent post-treatment strength and stiffness parameters that are estimated from homogenization theories, assuming the bulbs as rigid inclusions.

One of the most important design parameters is the volume replacement ratio. It represents the volumetric incidence of the ground treatment. It can be defined as:

$$R_s = \frac{G_T}{A} \quad (8)$$

where G_T is the grout take, i.e. the volume of grout injected per unit depth, and A is the area of the unit cell. The volume replacement ratio, R_s , can be conveniently expressed as a percentage or in l/m^3 . For example, considering a square grid with hole spacing of 3.0 x 3.0 m and a grout take of 800

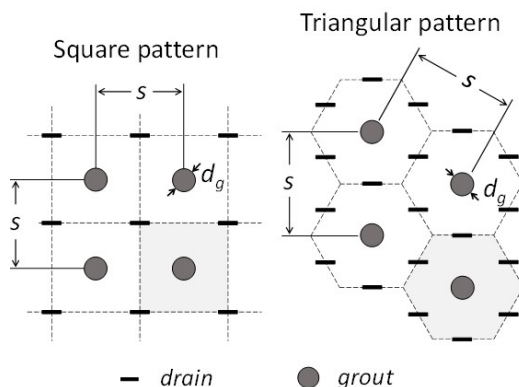


Figure 45. Typical *CPR* grouting layout plans. The area of the unit cell is shaded.

l/m , the volume replacement ratio is $R_s = 89 l/m^3 = 8.9\%$. Modeling the grout bulb as an equivalent cylinder, its diameter is $d_g = \sqrt{4G_T / \pi} = 101$ cm. As a rule of thumb, the grid spacing can be approximated to two- or three-times the grout bulb diameter.

A combination of in situ tests is strongly recommended to assess the degree of ground improvement. *SPT*, *CPT*, and pressuremeter tests must be used with caution because their results are highly dependent on test location, but can be checked by measuring the shear wave velocity. Seismic testing can provide a macro-scale assessment of grouting effectiveness by analyzing wave propagation characteristics pre- and post-treatment. Successful examples using seismic surface wave analysis to assess the efficiency of *CPR* grouting are reported in Cirone et al. (2017) and Park et al. (2018).

Two cases of special interest will be summarized in the next section, both in the city of Rio de Janeiro.

9.3 Athletes Park

CPR Grouting was used in the construction of Athletes Park located in the Barra da Tijuca district (Riccio Filho et al., 2013). Soil conditions at the site consisted of large deposits of very soft organic clay, up to 10 m thick, underlain by dense sands. Two different engineering solutions were chosen: soft soil of up to a depth of 3 m was replaced; *CPR* grouting was applied in the remaining areas (approximately 16,000 m^2 treated in less than two months) where the soft soil was in the range 4 – 10m thick. Field tests, comprising *CPTu* and vane shear tests, showed extremely low values of undrained strength, as low as 3 kPa up to 6 m depth. Shelby samples tested in the laboratory exhibited very high compressibility, so the expected total settlement was 1.2 m for a 2.2 m high earth fill embankment with no ground treatment.

CPR grouting began with the installation of vertical drains in a square grid pattern, with spacing of 1.5 m. Next, grout was injected into holes in a 3.0 x 3.0 m square grid. The bottom-up method was adopted. The following criteria were established: 800-1000 l/m for the grout take and 1000 kPa for the pressure. Figure 46 shows the grout injection being executed over the pre-installed grid of vertical drains.

To assess the performance of the ground treatment, several pressuremeter tests were conducted, comparing the pre-treatment and post-treatment results. A total of 15 settlement plates were installed and monitored during a period of 3.5 months. Most of the plate readings showed rapid settlement stabilization after the embankment had reached its final height of 2.2 m, with settlements less than 120 mm. The overall project performance was considered quite satisfactory, although the observational time was limited.

9.4 Recreio dos Bandeirantes.

The ground treatment at the Recreio dos Bandeirantes is an interesting one because it applied the homogeneous



Figure 46. Ground improvement at the Athletes Park by means of CPR grouting. Courtesy of Engegraut Ltda.

medium method to a real case consisting of an embankment on soft soil treated with CPR grouting. The study is described in detail by Riccio Filho et al. (2020) and a short summary is presented here.

The Recreio dos Bandeirantes district, in the western side of Rio de Janeiro, is a region well known for the presence of soft soil deposits. At the site, CPR grouting was carried out in an 8.0m-thick soft soil layer, to reduce settlement and consolidation time due to the loading imposed by a 2.0 m high embankment. Drains were installed in a triangular grid pattern with 1.5 m spacing, and grout injection points were spaced 3.0 m apart. The grout take was 1100 l/m.

An estimate of the improvement factor could be made on the basis of the settlement curves presented in Figure 47. The final settlement for the condition without CPR grouting ($s = 1.06$ m) was calculated using the oedometric method and the data from the site investigations. Settlement with PVDs was predicted considering a triangular pattern with a spacing equal to 1.5 m. The final settlement of the CPR grouting improved soil ($s = 0.167$ m) was obtained by extrapolating the settlement plate readings with Asaoka’s method. Comparing the curves revealed that CPR grouting was capable of accelerating the time for settlement stabilization (90% degree of consolidation was achieved in 175 days) and providing an improvement factor of about $1.06/0.167 = 6.3$.

9.5 Final remarks

The practice experience in Brazil with soft soil improvement using CPR Grouting permitted the following conclusions:

CPR grouting is an effective technique for ground improvement of soft clays. Recent research improved the theoretical understanding of the technique, however there is still no acceptance of its effectiveness among many geotechnical engineers. The development of a systematic approach for design, execution, monitoring and control will mark the acceptance of CPR grouting as a technique for treatment of soft clays.

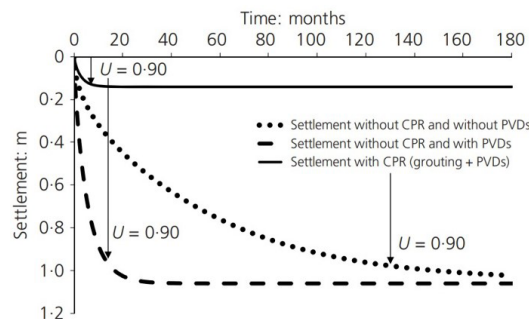


Figure 47. Comparison of settlement vs time curves at Recreio dos Bandeirantes (Riccio Filho et al., 2020).

Table 6. Typical range of β values as a function of soft soil improvement techniques.

Soft soil improvement technique	Typical range of β values
With or without drains or basal reinforcement (<i>UE/RE</i>)	1.0
Granular stone columns (<i>VSC</i>)	1.5 to 3.0
Geosynthetic encased granular columns (<i>GEC</i>)	2 to 4
Shallow soil mixing (<i>SSM</i>) and CPR grouting	5 to 10 (*)
Piled embankments (<i>PE</i> or <i>DSM</i>)	(**)

(*) range based on limited literature information. (**) β very high, not adopted.

10. Soft soil improvement techniques: settlement behavior

Based on the literature and the results presented in this paper, ranges of settlement improvement factor values, β , were obtained for the soft soil improvement techniques discussed here, as shown in Table 6. It is observed that as the degree of ground improvement increases the soft foundation gets stiffer and the parameter better increases proportionally. Piled embankments (*PE* or *DSM*) present settlements at least an order of magnitude smaller than other soft soil improvement techniques. Therefore, in this case it is not common to use the β variable to quantify the improvement of settlements, but then the load transfer Efficiency (BS, 2012) is the key design parameter. The consequence of lower settlements, or an increase in the value of β , is a lower required volume of fill and the related environmental benefits.

11. Conclusions

This paper has summarized recent studies related to the application of different soft ground improvement techniques mainly in the context of Brazilian soft clays.

Vacuum consolidation, the first technique discussed, is a highly efficient technique used worldwide for the improvement of soft soils. Even though the study at the Rio de Janeiro site described here presented low efficiency, the technique can and should be used with Brazilian soft clays, however with

better technological control and closer monitoring in order to achieve the necessary efficiency results.

This paper presented and discussed in sequence the different techniques for soft clay improvement that promote the strengthening of the soil, either by means of column-like elements (*VSC*, *GEC*, *PE/DSM*) or by incorporating cement (*SSM*) or mortar (*CPR*) mixtures into the soft soil.

Common to all techniques is that settlements decrease with increasing strengthening of the soft soil. The settlement improvement factor β , that relates the settlements with and without treatment of the soft soil, is a good way to rank the various improvement techniques discussed here.

The comparison of the reinforced embankment *RE* (*TE1*) with the embankment built on geosynthetic encased columns *GEC* (*TE2*) presented in section 5 showed that for the same settlement value in both cases, the *GEC* permitted an applied vertical stress 2.5 times greater than the reinforced embankment. The *GEC* technique has proven to be even more efficient when the comparison is made for horizontal displacements.

The results presented throughout the paper showed that the improvement of soft soils generally results in a decrease in construction time. Granular columns (*VSC* or *GEC*) act as large drains and generally accelerate settlements substantially compared to using prefabricated vertical drains. In the other techniques presented here (*CPR*, *SSM*, *PE/DSM*) the construction times are dictated primarily by the execution time of the technique itself, since the stabilization of settlements after the execution of the landfill is relatively fast, in general a matter of days or a few months. In any soft soil improvement technique, temporary surcharge is used to reduce post-construction settlements.

The literature shows that soft ground treatment using column-like elements or soil-binder mixtures is usually governed by service limit state conditions rather than by ultimate limit state conditions. In line with this, this paper has given more emphasis to settlement control rather than to stability control, although the latter must also be carefully assessed in design. The clear differences in safety factor values from stability analyses of embankments with and without soft soil improvement, presented in sections 4 and 5 respectively for the *VSC* and *GEC* techniques, confirm this.

Other important factors to be verified in design are, for example, negative friction and lateral embankment load in column-like elements of piled embankments (*PE* or *DSM*), which were outside the scope of this paper.

Acknowledgements

The various studies presented here would not have been possible without the support of the funding agencies, the Coordination for the Improvement of Higher Education Personnel (Capes) of the Ministry of Education (MEC), the National Council for Scientific and Technological Development (CNPq) of the Ministry of Science, Technology and Innovation

(MCTI), and the Research Support Foundation of the State of Rio de Janeiro - FAPERJ, as well as the companies involved. The authors recognize the important support of Talytha Fonte Boa in editing the final version of the article.

Declaration of interest

The authors have no conflicts of interest to declare. All co-authors have observed and affirmed the contents of the paper and there is no financial interest to report.

Authors' contributions

Marcio de Souza Soares de Almeida: overall conceptualization, planning and organization, writing – abstract, intro and conclusion, plus coordination and critical review of sections written by collaborators. Maria Esther Soares Marques: writing of one section, critical analysis and review entire paper. Diego de Freitas Fagundes, Mário Riccio and Uberescilas Fernandes Polido: section writing and review of sections written by the others. Alessandro Cirone, Bruno Teixeira Lima and Iman Hosseinpour: writing of sections. All authors provided comments to the final version of the paper.

Data availability

The data used for the production of this paper can be found in the following references that are listed in the references section of this paper: Marques & Leroueil (2015), Freitas (2021), Almeida et al. (2013, 2014, 2018b), Almeida (2019), Hosseinpour et al. (2015, 2016), Machado (2016), Assis (2016), Ávila (2021), Nascimento (2016), França et al. (2016), Cirone (2016), Cirone et al. (2017), and Riccio Filho et al. (2020, 2022).

List of acronyms

<i>CAU</i>	Anisotropic triaxial test
COPPE-UFRJ	Instituto Alberto Luiz Coimbra de Pós-Graduação e Pesquisa em Engenharia of the Federal University of Rio de Janeiro
<i>COV</i>	Covariance
<i>CP</i>	Cell pressure
<i>CPR</i>	Deep radial consolidation (Consolidação Profunda Radial)
<i>CPT</i>	Cone penetration test
<i>CPTu</i>	Piezocone Test
<i>CR</i>	Compression ratio
<i>DSM</i>	Deep Soil Mixing
<i>ESP</i>	Effective Stress Path
<i>EX</i>	Extensometer
<i>FEM</i>	Finite element method.
<i>GEC</i>	Geosynthetic encased column

<i>GECl</i>	Test embankment	<i>J1x</i>	Secant stiffness of the GR PP25 in x direction
<i>GR</i>	Geosynthetic reinforcement	<i>J1y</i>	Secant stiffness of the GR PP25 in y direction
<i>GWT</i>	Ground water table	<i>J2</i>	Secant stiffness of the GR PP60
<i>HPG</i>	Horizontal profilometer gauges	<i>K_{onc}</i>	Coefficient of earth pressure at rest of a normally consolidated clay
<i>IN, I</i>	Inclinometer	<i>K*</i>	Coefficient of earth pressure after stone column installation.
<i>OCR</i>	Overconsolidation ratio	<i>n</i>	Stress concentration factor
<i>OMC</i>	Organic matter content	<i>N_{spt}</i>	SPT blow count
<i>PVD</i>	Prefabricated Vertical Drain	<i>p'</i>	Mean effective stress
<i>PZ</i>	Piezometer	<i>P</i>	Piezometer
<i>RE</i>	Reinforced embankment	<i>PI</i>	Plasticity index
<i>REI</i>	Reinforced test embankment	<i>pH</i>	Potential of hydrogen
<i>SLS</i>	Serviceability Limit State	<i>q</i>	Deviator Stress
<i>SP, S, PR</i>	Settlement plate	<i>q</i>	Vertical stress (surcharge) applied to the embankment surface
<i>SPT</i>	Standard Penetration Test	<i>q_c</i>	Tip resistance from CPT
<i>SS</i>	Settlement sensor	<i>q_t</i>	Corrected tip resistance from CPT
<i>SSM</i>	Shallow soil mixing	<i>q_u</i>	Unconfined compressive strength
<i>UCT</i>	Unconfined compression test	<i>q_{uF}</i>	Unconfined compressive strength of field samples
<i>UE</i>	Unreinforced embankment	<i>q_{uL}</i>	Unconfined compressive strength of laboratory samples
<i>ULS</i>	Ultimate Limit State	<i>RS</i>	Replacement Ratio
<i>VP</i>	Vacuum pump	<i>s</i>	Centre to centre pile spacing
<i>VSC</i>	Vibro replacement	<i>S</i>	Surface settlement point
<i>VST</i>	Vane shear test	<i>S_u</i>	Undrained shear strength

List of symbols

<i>A</i>	Influence area of column	<i>s</i>	Centre to centre pile spacing
<i>A_c</i>	Cross sectional area of a column	<i>S</i>	Surface settlement point
<i>a_c</i>	Area replacement ratio	<i>S_u</i>	Undrained shear strength
<i>B</i>	Membrane effect	<i>S_d</i>	Standard deviation
<i>C</i>	Soil reaction	<i>s'</i>	Geometric parameter
<i>C_c</i>	Compression index	<i>t</i>	Time
<i>C_s</i>	Swelling index	<i>T</i>	Tensile force
<i>c_v</i>	Vertical consolidation coefficient	<i>T_{max}</i>	Maximum tensile force
<i>d</i>	Pile diameter, pile size or pile cap size	<i>T_u</i>	Geosynthetic ultimate tensile strength
<i>d_c</i>	Column diameter	<i>w</i>	Natural water content
<i>d_e</i>	Diameter of influence	<i>w_p</i>	Plastic limit
<i>dg</i>	Equivalent diameter of grout bulb	<i>w_l</i>	Liquid limit
<i>DR</i>	Ratio between maximum horizontal δh and maximum vertical displacements Δh ($DR = \delta h / \Delta h$)	<i>z</i>	Orthogonal maximum deflection of the geosynthetic
<i>E</i>	Efficiency of the load transfer mechanism	<i>z_d</i>	Diagonal maximum deflection of the geosynthetic
<i>E_{impr}</i>	Efficiency improvement	α	Area replacement ratio
<i>E_{max}</i>	Maximum load efficiency	β	Settlement improvement factor ($\beta = \Delta h / \Delta h_c$)
<i>EP</i>	Earth pressure cell with integrated piezometer	γ	Unit weight of the embankment fill material
<i>e₀</i>	Initial void ratio	γ_s	Unit weight of solids
<i>E_{s50}</i>	Secant modulus at 50% strength	Δh	settlement or maximum settlement without columns
<i>F</i>	Vertical pile load	Δh_c	settlement with columns
<i>f_{ck,28}</i>	Characteristic unconfined compressive strength at 28 days	Δu	Differential settlement at the top of embankment
<i>G_T</i>	Grout take, liters/m	$\Delta \omega$	Simulated settlement of the subsoil using the mobile tray
<i>GR</i>	geosynthetic reinforcement	μ	Bjerrum (1973) correction factor
<i>H</i>	Embankment height	σ_v	Vertical stress
<i>H_{crit}</i>	Critical height	σ_{vc}	Vertical stress on the top of column
<i>I</i>	Inclinometer	σ_{vs}	Vertical Stress on the top of soil
<i>J</i>	Geosynthetic secant stiffness modulus	ϕ'	Effective soil friction angle

References

- Almeida, M.S.S., Lima, B.T., Riccio, M.V.F., Jud, H., Almeida, M.C.F., & Roza, F. (2014). Stone columns field test: monitoring data and numerical analyses. *Geotechnical Engineering Journal of the SEAGS and AGSSEA*, 45(1), 103-112.
- Almeida, M.S.S., & Marques, M.E.S. (2013). *Design and performance of embankments on very soft soils*. London: CRC Press.
- Almeida, M.S.S., Marques, M.E.S., Lima, B.T., & Alvez, F. (2008). Failure of a reinforced embankment an extremely soft peat clay layer. In *Eurogeo4* (Vol. 1, pp. 1-8), Scotland.
- Almeida, M.S.S. (2015). Amélioration des sols compressibles: études en vraie grandeur, modèles physiques et numériques. In *Conférence Coulomb*, Paris. Retrieved in July 26, 2022, from <https://www.cfms-sols.org/manifestations/conference-coulomb>
- Almeida, M.S.S. (2019). Soft ground improvement: field and numerical studies. In *XVI Pan-American Conference on Soil Mechanics and Geotechnical Engineering* (Keynote Lecture of Technical Session, No. 5, "Soft soils"), Cancun, Mexico.
- Almeida, M.S.S., Fagundes, D.F., Almeida, M.C.F., Hartmann, D.A., Giroult, R., Thorell, L., & Blanc, M. (2018a). Load transfer mechanism of reinforced piled embankments. In *Physical Modelling in Geotechnics - ICPMG18* (Vol. 2, pp. 1031-1036). London: CRC Press.
- Almeida, M.S.S., Riccio Filho, M., Hosseinpour, I., & Alexiew, D. (2018b). *Geosynthetic encased columns for soft soil improvement*. London: CRC Press. <http://dx.doi.org/10.1201/9781315177144>.
- Almeida, M.S.S., Fagundes, D.F., Thorel, L., & Blanc, M. (2020). Geosynthetic-reinforced pile-embankments: numerical, analytical and centrifuge modelling. *Geosynthetics International*, 27(3), 301-314. <http://dx.doi.org/10.1680/jgein.19.00011>.
- Almeida, M.S.S., Hosseinpour, I., & Riccio, M. (2013). Performance of a geosynthetic-encased column (GEC) in soft ground: numerical and analytical studies. *Geosynthetics International*, 20(4), 252-262. <http://dx.doi.org/10.1680/jgein.13.00015>.
- Almeida, M.S.S., Hosseinpour, I., Riccio, M., & Alexiew, D. (2015). Behavior of geotextile-encased granular columns supporting test embankment on soft deposit. *Journal of Geotechnical and Geoenvironmental Engineering*, 141(3), 04014116. [http://dx.doi.org/10.1061/\(ASCE\)GT.1943-5606.0001256](http://dx.doi.org/10.1061/(ASCE)GT.1943-5606.0001256).
- Almeida, M.S.S., Deotti, L., Almeida, M.C.F., Marques, M.E.S., & Cardoso, I.M. (2021). Vacuum preloading on structured clay: field, laboratory and numerical studies. *International Journal of Geomechanics*, 1(10), 21. [http://dx.doi.org/10.1061/\(ASCE\)GM.1943-5622.0002170](http://dx.doi.org/10.1061/(ASCE)GM.1943-5622.0002170).
- Andrade, G.F.S.M., Lima, B.T., & Seira, A.C.C.F. (2022). Laboratory investigation of geogroup inclusion: the influence of the substitution ratio. *Proceedings of the Institution of Civil Engineers - Ground Improvement*. In press. <http://dx.doi.org/10.1680/jgrim.21.00009>.
- Andrade, G.G., Lopes, A.N., Antunes, R.P., & Dias, D.R. (2010). Experiências Brasileiras com estabilização de solos moles saturados através de sistema Dry-Mix – STABTEC. In *Anais do XV Congresso Brasileiro de Mecânica dos Solos e Engenharia Geotécnica* (pp. 1-6), Gramado. ABMS, CBMR, ISRM and SPG (in Portuguese).
- Assis, V.C. (2016). *Structured embankment on soft soil over DSM columns* [Master's dissertation]. Federal University of Rio de Janeiro repository (in Portuguese). Retrieved in July 26, 2022, from <http://www.coc.ufrj.br/pt/dissertacoes-de-mestrado/389-msc-pt-2016/4696-vincius-cardoso-de-assis>
- Au, S.K.A., Yeung, A.T., Soga, K., & Cheng, Y.M. (2007). Effects of subsurface cavity expansion in clays. *Geotechnique*, 57(10), 821-830. <http://dx.doi.org/10.1680/geot.2007.57.10.821>.
- Au, S.K.A., Soga, K., Jafari, M.R., Bolton, M.D., & Komiya, K. (2003). Factors affecting long-term efficiency of compensation grouting in clays. *Journal of Geotechnical and Geoenvironmental Engineering*, 129(3), 254-262. [http://dx.doi.org/10.1061/\(ASCE\)1090-0241\(2003\)129:3\(254\)](http://dx.doi.org/10.1061/(ASCE)1090-0241(2003)129:3(254)).
- Ávila, C.T.B. (2021). *Structured embankment over columns with soil cement mixture* [Master's dissertation]. Federal University of Juiz de Fora repository (in Portuguese). Retrieved in July 26, 2022, from <https://www2.ufrj.br/pec/wp-content/uploads/sites/115/2022/02/Disserta%C3%A7%C3%A3o-102470031.pdf>
- Baroni, M., & Almeida, M.S.S. (2022). Undrained shear strength correlation analysis based on vane tests in the Jacarepaguá Lowlands, Brazil. *Soils and Rocks*, 45(2), e2022072721. <http://dx.doi.org/10.28927/SR.2022.072721>.
- Baroni, M., & Almeida, M. (2017). Compressibility and stress history of very soft organic clays. *Geotechnical Engineering*, 170(2), 148-160. <http://dx.doi.org/10.1680/jgeen.16.00146>.
- Barron, R.A. (1948). Consolidation of fine-grained soils by drain wells. *Transactions of the American Society of Civil Engineers*, 113(1), 718-724.
- Besançon, G., Iorio, J.P., & Soyezet, B. (1984). Analyse des paramètres de calcul intervenant dans le dimensionnement des colonnes ballastées. In *Renforcement en Place des Sols et des Roches: Comptes Rendus du Colloque International* (pp. 119-126), Paris.
- Bjerrum, L. (1973). Problems of soil mechanics and construction on soft clays and structurally instable soils. In *Proceedings of the 8th International Conference on Soil Mechanics and Foundation Engineering* (Vol. 3, pp. 111-159), Moscow.
- Blanc, M., Rault, G., Thorel, L., & Almeida, M.S.S. (2013). Centrifuge investigation of load transfer mechanisms in a granular mattress above a rigid inclusions network.

- Geotextiles and Geomembranes*, 36, 92-105. <http://dx.doi.org/10.1016/j.geotexmem.2012.12.001>.
- Blanc, M., Thorel, L., Girout, R., & Almeida, M.S.S. (2014). Geosynthetic reinforcement of a granular load transfer platform above rigid inclusions: comparison between centrifuge testing and analytical modelling. *Geosynthetics International*, 21(1), 37-52. <http://dx.doi.org/10.1680/gein.13.00033>.
- Blanc, M., Thorel, L., Girout, R., Almeida, M.S.S., & Fagundes, D.F. (2018). Load transfer mechanism of piled embankments: centrifuge tests versus analytical models. In *Proceedings of the 9th International Conference on Physical Modelling in Geotechnics* (Vol. 1, pp. 1043-1048). London: CRC Press.
- BS 8006. (2012). *Code of practice for strengthened/reinforced soils and other fills, incorporating Corrigendum 1*. British Standards Institution, London.
- BS 8006-1. (2017). *Code of practice for strengthened/reinforced soils and others fills*. British Standards Institution, London.
- Cardoso, I.M. (2021). *Vacuum Preloading as a solution for construction on soft soils* [Master's dissertation]. Federal University of Rio de Janeiro' repository (in Portuguese). Retrieved in July 26, 2022, from <http://www.coc.ufrj.br/pt/dissertacoes-de-mestrado/635-2021/9865-igor-medeiros-cardoso>
- Cirone, A. (2016). *Geotechnical modeling of CPR grouting* [Master's dissertation]. Politecnico di Milano' repository. Retrieved in July 26, 2022, from <https://www.politesi.polimi.it/handle/10589/120023>
- Cirone, A., Rodrigues, R., & Park, C. (2017). MASW control of grouting. In *SEG Technical Program Expanded Abstracts 2017* (pp. 5228-5232). Houston: Society of Exploration Geophysicists. <http://dx.doi.org/10.1190/segam2017-17740142.1>.
- Chai, J.C., Ong, C.Y., Carter, J.P., & Bergado, D.T. (2013). Lateral displacement under combined vacuum pressure and embankment loading. *Geotechnique*, 63(10), 842-856. <http://dx.doi.org/10.1680/geot.12.P060>.
- Choa, V. (1989). Drains and vacuum preloading pilot test. In *Proceedings of the 12th International Conference on Soil Mechanics and Foundation Engineering* (pp. 1347-1350), Rio de Janeiro.
- CUR 226 (2016). *Ontwerprichtlijn paalmatrassystemen* [Design guideline piled embankments]. Stichting CUR, Gouda, Netherlands (in Dutch).
- EBGEO. (2011). *Recommendations for design and analysis of earth structures using geosynthetic reinforcements*. Deutsche Gesellschaft für Geotechnik e.V. (DGGT), Berlin.
- EN 14679. (2005). *Execution of special geotechnical works: deep mixing*. European Standard, London.
- EuroSoilStab. (2002). *CT97-0351: development of design and construction methods to stabilize soft organic soils: design guide for soft soil stabilization*. European Commission, Industrial and Materials Technologies Program, Watford, UK.
- Fagundes, D.F., Almeida, M.S.S., Girout, R., Blanc, M., & Thorel, L. (2015). Behaviour of piled embankment without reinforcement. *Geotechnical Engineering*, 168(6), 514-525. <http://dx.doi.org/10.1680/jgeen.14.00155>.
- Fagundes, D.F., Almeida, M.S.S., Thorel, L., & Blanc, M. (2017). Load transfer mechanism and deformation of reinforced piled embankments. *Geotextiles and Geomembranes*, 45(2), 1-10. <http://dx.doi.org/10.1016/j.geotexmem.2016.11.002>.
- FHWA. (1983). *Design and construction of stone columns* (Report, No. FHWA/RD-83/027, Vol. 1). FHWA, Washington.
- FHWA-HRT-13-046. (2013). *Deep mixing for embankment and foundation support* (Federal Highway Administration Design Manual, No. FHWA-HRT-13-046). FHWA, Washington.
- Forsman, J., Jyrävä, H., Lahtinen, P., Niemelin, T., & Hyvönen, I. (2015). *Mass stabilization manual*. Retrieved in July 23, 2022, from <https://nzstirrers.com/wp-content/uploads/2014/02/ALLU-Ramboll-Mass-Stabilisation-Ma-1.pdf>
- França, H.F., Polido, U.F., Nascimento, T.Z., & Lemos, S.G.F.P. (2016). Estabilização de solo mole por mistura de cimento em área da Barra da Tijuca, RJ: estudo de caso. In *Anais do 17º Congresso Brasileiro de Mecânica dos Solos e Engenharia Geotécnica*, Belo Horizonte. ABMS, CBMR, ISRM and SPG (in Portuguese). <http://dx.doi.org/10.20906/CPS/CB-03-0021>.
- Freitas, M.D.S. (2021). *Técnica de vácuo em solos moles aplicada a infraestrutura de transportes* [Master's dissertation]. Military Institute of Engineering (in Portuguese). Retrieved in July 23, 2022, from https://sucupira.capes.gov.br/sucupira/public/consultas/coleta/trabalhoConclusao/viewTrabalhoConclusao.jsf?popup=true&id_trabalho=11152264
- Girout, R., Blanc, M., Thorel, L., Fagundes, D.F., & Almeida, M.S.S. (2016). Arching and deformation in a piled embankment: centrifuge tests compared to analytical calculations. *Journal of Geotechnical and Geoenvironmental Engineering*, 142(12), 04016069. [http://dx.doi.org/10.1061/\(ASCE\)GT.1943-5606.0001557](http://dx.doi.org/10.1061/(ASCE)GT.1943-5606.0001557).
- Han, J., & Ye, S.L. (2002). A theoretical solution for consolidation rates of stone column reinforced foundations accounting for smear and well resistance effects. *International Journal of Geomechanics*, 2(2), 135-151. [http://dx.doi.org/10.1061/\(ASCE\)1532-3641\(2002\)2:2\(135\)](http://dx.doi.org/10.1061/(ASCE)1532-3641(2002)2:2(135)).
- Hartmann, D.A., Almeida, M.C.F., Almeida, M.S.S., Blanc, M., & Thorel, L. (2014). On the influence of pretension and number of geosynthetic layers on piled embankment performance. In *Proceedings of the 10th International Conference on Geosynthetics - ICG 2014*, Berlin, Germany.

- Harvey, J.A.F. (1997). Vacuum drainage to accelerate submarine consolidation at Chek Lap Kok, Hongkong. *Ground Engineering*, 1997(30), 34-36.
- Hosseinpour, I., Almeida, M.S.S., & Riccio, M. (2015). Full-scale load test and finite-element analysis of soft ground improved by geotextile-encased granular columns. *Geosynthetics International*, 22(6), 428-438. <http://dx.doi.org/10.1680/jgein.15.00023>.
- Hosseinpour, I., Almeida, M.S.S., Riccio, M.V.F. (2016). Ground improvement of soft soil by geotextile-encased columns. *Proceedings of the ICE - Ground Improvement*, 169, 297-305.
- Indraratna, B. (2010). Recent advances in the application of vertical drains and vacuum preloading in soft soil stabilization. *Australian Geomechanics Journal*, 45(2), 1-43.
- Jacob, A., Thevanayagam, S., & Kavazanjian, E. (1994). Vacuum-assisted consolidation of a hydraulic landfill. In *Proceedings of the Conference on Vertical and Horizontal Deformations of Foundations and Embankments* (Geotechnical Special Publication, No. 40, pp. 1249-1261). ASCE.
- Kempfert, H.-G., Gobel, C., Alexiew, D., & Heitz, C. (2004). German recommendations for reinforced embankments on pile-similar elements. In *Proceedings of the 3rd European Geosynthetics Conference* (pp. 279-284), Munich.
- Kitazume, M., & Terashi, M. (2013). *The deep mixing method*. Boca Raton: CRC Press. <http://dx.doi.org/10.1201/b13873>.
- Kjellman, W. (1952). Consolidation of clay soil by means of atmospheric pressure. In *Proceedings of the Conference on Soil Stabilization* (pp. 258-263). Cambridge: MIT.
- Komiya, K., Soga, K., Akagi, H., Jafari, M.R., & Bolton, M.D. (2001). Soil consolidation associated with grouting during shield tunneling in soft clayey ground. *Geotechnique*, 51(10), 835-846. <http://dx.doi.org/10.1680/geot.2001.51.10.835>.
- Lemos, S.G.F.P., Almeida, M.S.S., Consoli, N.C., Nascimento, T.Z., & Polido, U.F. (2020). Field and laboratory investigation of highly organic clay stabilized with Portland cement. *Journal of Materials in Civil Engineering*, 32(4), 04020063. [http://dx.doi.org/10.1061/\(ASCE\)MT.1943-5533.0003111](http://dx.doi.org/10.1061/(ASCE)MT.1943-5533.0003111).
- Lima, B.T. (2012). *Study of the use of stone columns on very soft clayey soils* [Doctoral thesis]. Federal University of Rio de Janeiro repository (in Portuguese). Retrieved in July 23, 2022, from <http://www.coc.ufrj.br/pt/teses-de-doutorado/156-2012/4103-bruno-teixeira-lima>
- Lima, B.T., Almeida, M.S.S., & Hosseinpour, I. (2019). Field measured and simulated performance of a stone columns-strengthened soft clay deposit. *International Journal of Geotechnical Engineering*, 16(6), 776-785. <http://dx.doi.org/10.1080/19386362.2019.1653506>.
- López-Acosta, N.P., Espinosa-Santiago, A.L., Pineda-Núñez, V.M., Ossa, A., Mendoza, M.J., Ovando-Shelley, E., & Botero, E. (2019). Performance of a test embankment on very soft clayey soil improved with drain-to-drain vacuum preloading technology. *Geotextiles and Geomembranes*, 47(5), 618-631. <http://dx.doi.org/10.1016/j.geotextmem.2019.103459>.
- Machado, M.C.B. (2016). *Treatment of clayey soft soils by cement mixtures in deep* [Master's dissertation]. Federal University of Rio de Janeiro repository (in Portuguese). Retrieved in July 23, 2022, from <http://www.coc.ufrj.br/pt/dissertacoes-de-mestrado/389-msc-pt-2016/4683-michelle-christini-de-brito-machado>
- Magnani, H.O., Ehrlich, M., & Almeida, M.S.S. (2010). Embankments over soft clay deposits: contribution of basal reinforcement and surface sand layer to stability. *Journal of Geotechnical and Geoenvironmental Engineering*, 136(1), 260-264. [http://dx.doi.org/10.1061/\(ASCE\)GT.1943-5606.0000200](http://dx.doi.org/10.1061/(ASCE)GT.1943-5606.0000200).
- Marques, M.E.S., & Leroueil, S. (2015). Vacuum consolidation and vacuum consolidation with heating. In B. Indraratna, J. Chu & C. Rujikiatkamjorn (Eds.), *Ground improvement series: chemical, electrokinetic, thermal and bioengineering* (Vol. 3, pp. 537-554). Amsterdam: Elsevier. <http://dx.doi.org/10.1016/B978-0-08-100191-2.00017-4>.
- Marques, M.E.S., Lima, B.T., Oliveira, J.R.M., Antoniutti Neto, L., & Almeida, M.S.S. (2008). Geotechnical characterization of a compressible soil of Itaguaí, Rio de Janeiro. In *IV Proceedings of the Luso Brazilian Geotechnical Congress*, Coimbra. CD-ROM (in Portuguese).
- Massarsch, K.R., & Topolnicki, M. (2005). Regional report: European practice of soil mixing technology. In *Proceedings of the International Conference on Deep Mixing – Best Practice and Recent Advances*, Stockholm.
- McCabe, B.A., Nimmons, G.J., & Egan, D. (2009). A review of field performance of stone columns in soft soils. *Geotechnical Engineering*, 162(6), 323-334. <http://dx.doi.org/10.1680/geng.2009.162.6.323>.
- McGuire, M., Sloan, J., Collin, J., Filz, G., 2012, Critical Height of Column-Supported embankments from Bench-Scale and Field-Scale Tests. In *ISSMGE - TC 211 International Symposium on Ground Improvement IS-GI* Brussels.
- Nascimento, T.Z. (2016). *Laboratory and field behavior of a cement stabilized very soft clay* [Master's dissertation]. Federal University of Rio de Janeiro's repository (in Portuguese). Retrieved in July 23, 2022, from <http://www.coc.ufrj.br/pt/dissertacoes-de-mestrado/389-msc-pt-2016/4695-tayro-zonta-nascimento>
- Park, C., Richter, J., Rodrigues, R., & Cirone, A. (2018). MASW applications for road construction and maintenance. *The Leading Edge*, 37(10), 724-730. <http://dx.doi.org/10.1190/tle37100724.1>.
- Pinto, C.S., Almeida, M.S.S., Almeida, M.C.F., Jenck, O., Briacom, L., Houda, M., & Emeriault, F. (2014). Physical model studies on piled embankments with and without geosynthetics. In *Proceedings of the 10 th International Conference on Geosynthetics - ICG 2014*, Berlin.

- Priebe, H.J. (1995). *The design of vibro replacement* (pp. 31-37). London: Ground Engineering. Retrieved in July 23, 2022, from <https://www.geplus.co.uk/technical-paper/technical-paper-the-design-of-vibro-replacement-01-12-1995/>
- Qian, J.H., Zhao, W.B., Cheung, Y.K., & Lee, P.K.K. (1992). The theory and practice of vacuum preloading. *Computers and Geotechnics*, 13(2), 103-118. [http://dx.doi.org/10.1016/0266-352X\(92\)90027-Q](http://dx.doi.org/10.1016/0266-352X(92)90027-Q).
- Raithel, M., & Kempfert, H.G. (2000). Calculation models for dam foundations with geotextile coated sand column. In *Proceedings of the ISRM International Symposium* (pp. 347-352), Melbourne, Australia.
- Riccio Filho, M.V., Baroni, M., & Almeida, M.S.S. (2013). Ground improvement in soft soils in Rio de Janeiro: the case of Athletics Park. *Proceedings of the Institution of Civil Engineers. Civil Engineering*, 166(6), 36-43. <http://dx.doi.org/10.1680/cien.13.00008>.
- Riccio Filho, M.V., Cirone, A., Almeida, M.S.S., Rodriguez, T.T., & Faria, D.A. (2020). Site investigation and performance of radial deep consolidation grouting in soft soil. *Proceedings of the Institution of Civil Engineers – Ground Improvement*, 173(1), 28-39. <http://dx.doi.org/10.1680/jgrim.18.00036>.
- Riccio Filho, M.V., Almeida, M.S.S., Vasconcelos, S.M., Pires, L.G.S., & Nicodemos, L.F. (2022). Embankment supported by low area replacement ratio stone columns, monitoring and numerical studies. *KSCE Journal of Civil Engineering*, 26(2), 619-629. <http://dx.doi.org/10.1007/s12205-021-0540-9>.
- Roza, F.C. (2012). *Behavior of works on soft soils with stone columns* [Master's dissertation]. Federal University of Rio de Janeiro repository (in Portuguese). Retrieved in July 26, 2022, from <http://www.coc.ufrj.br/pt/dissertacoes-de-mestrado/112-msc-pt-2012/4130-felipe-costa-roza>
- Rujikiatkamjorn, C., Indraratna, B., & Chu, J. (2007). Numerical modelling of soft soil stabilized by vertical drains, combining surcharge and vacuum preloading for a storage yard. *Canadian Geotechnical Journal*, 44(3), 326-342. <http://dx.doi.org/10.1139/t06-124>.
- Saboya, F., Tibana, S., Reis, R.M., Fonte-Boa, T., Almeida, M.S.S., & Marques, M.E.S. (2021). Centrifuge modeling of soft soil reinforced with granular columns. *Geotechnical and Geological Engineering*, 39(4), 2955-2967. <http://dx.doi.org/10.1007/s10706-020-01671-1>.
- Sandroni, S.S. (2014). Deslocamentos observados por longo período em aterro sobre solo mole reforçado com colunas de brita. In *Anais do 17º Congresso Brasileiro de Mecânica dos Solos e Engenharia Geotécnica*, Goiânia, Brasil (in Portuguese).
- Springman, S.M., Laue, J., Askarinejad, A., & Gautray, J.N.F. (2012). On the design of ground improvement for embankments on soft ground. In *Proceedings of the International Conference on Ground Improvement and Ground Control: Transport Infrastructure Development and Natural Hazards Mitigation* (Vol. 1, pp. 67-83), Wollongong, Australia. http://dx.doi.org/10.3850/978-981-07-3559-3_101-0006.
- Tavenas, F., Mieussens, C., & Bourges, F. (1979). Lateral displacement in clay foundations under embankments. *Canadian Geotechnical Journal*, 16(3), 532-550. <http://dx.doi.org/10.1139/t79-059>.
- Topolnicki, M. (2012). Design and execution practice of wet Soil Mixing in Poland. In *Proceedings of the International Symposium on Deep Mixing and Admixture Stabilization* (pp. 195-202), Okinawa.
- Topolnicki, M. (2016). General overview and advances in Deep Soil Mixing. In *Proceedings of the XXIV Geotechnical Conference of Torino Design, Construction and Controls of Soil Improvement Systems* (pp. 25-26), Torino.
- van Eekelen, S.J.M., Bezuijen, A., & van Tol, A.F. (2013). An analytical model for arching in piled embankments. *Geotextiles and Geomembranes*, 39, 78-102. <http://dx.doi.org/10.1016/j.geotexmem.2013.07.005>.
- Wu, J.Y. (2005). Numerical study of radial ground improvement technology in soft clay. In *Proceedings of Computing in Civil Engineering* (pp. 1-10), Cancun, Mexico. ASCE.
- Zheng, G., Liu, J., Lei, H., Rahman, M.S., & Tan, Z. (2017). Improvement of very soft ground by a high-efficiency vacuum preloading method: a case study. *Marine Georesources and Geotechnology*, 35(5), 631-642. <http://dx.doi.org/10.1080/1064119X.2016.1215363>.